lipopolysaccharide in macrophages[22]. We observed no significant difference in the amount of mitochondrial DNA in the blood between TAC-operated *Dnase2a*$^{-/-}$ and *Dnase2a*$^{+/+}$ mice (data not shown), excluding a possibility that circulating mitochondrial DNA is causing most of the inflammatory responses mediated by TLR9. The mechanisms presented here do not require release of mitochondrial DNA from cardiomyocytes into extracellular space.

Increased levels of circulating proinflammatory cytokines are associated with disease progression and adverse outcomes in patients with chronic heart failure[1]. Mitochondrial DNA plays an important role in inducing and maintaining inflammation in the heart. This mechanism might work in many chronic non-infectious inflammation-related diseases such as atherosclerosis, metabolic syndrome and diabetes mellitus.

METHODS SUMMARY

Animal study. The study was performed under the supervision of the Animal Research Committee of Osaka University and in accordance with the Japanese Act on Welfare and Management of Animals (No. 105). The 12- to 14-week-old mice were subjected to TAC[5,23] and severe TAC using 26- and 27-gauge needles for aortic constriction, respectively.

Biochemical assays. The DNase II activity was determined by the single radial enzyme-diffusion method[24]. The mRNA levels were determined by quantitative PCR with reverse transcription (RT–PCR)[5].

Histological analysis. The antibodies used were anti-mouse CD45 (ANASPEC), CD68 (Serotec), Ly6G/6C (BD Pharmingen), CD3 (Abcam), DNA (Abcam), LAMP2a (Zymed), LC3 (ref. 25) and TLR9 (Santa-Cruz). The *in situ* hybridization analysis was performed using DIG RNA Labelling Kit and DIG Nucleic Acid Detection Kit (Roche Diagnostics). Hearts were embedded in LR White resin for immunoelectron microscopy[26]. Heart sections were incubated in PicoGreen (Molecular Probes) for 1 h. Twenty-four hours before TAC, mice were injected intraperitoneally with 250 μg of EdU every 2 h five times, and EdU was detected with a Click-iT EdU Alexa Fluor 488 Imaging Kit (Invitrogen).

***In vitro and in vivo* rescue experiments with the TLR9 inhibitor.** Cardiomyocytes[5] were pre-treated with 1 μg ml^{-1} inhibitory CpG (ODN2088) or control (ODN2088 control) oligodeoxynucleotides for 5 h and incubated with 20 nM CCCP or 50 μM isoproterenol for 24 h (ref. 20). The cells were loaded with tetramethylrhodamine ethyl ester (Molecular Probe) at 10 nM for 30 min. The mice were injected intravenously with 500 μg of the oligodeoxynucleotides 2 h before and 2 and 4 days after TAC, and every 3 days thereafter.

Statistical analysis. Results are shown as the mean ± s.e.m. Paired data were evaluated using a Student's *t*-test. A one-way analysis of variance with the Bonferroni post hoc test was used for multiple comparisons. The Kaplan–Meier method with a log-rank test was used for survival analysis.

Full Methods and any associated references are available in the online version of the paper at www.nature.com/nature.

Received 26 June 2011; accepted 1 March 2012.
Published online 25 April 2012.

1. Mann, D. L. Inflammatory mediators and the failing heart: past, present, and the foreseeable future. *Circ. Res.* **91,** 988–998 (2002).
2. Pollack, Y., Kasir, J., Shemer, R., Metzger, S. & Szyf, M. Methylation pattern of mouse mitochondrial DNA. *Nucleic Acids Res.* **12,** 4811–4824 (1984).
3. Cardon, L., Burge, C., Clayton, D. A. & Karlin, S. Pervasive CpG suppression in animal mitochondrial genomes. *Proc. Natl Acad. Sci. USA* **91,** 3799–3803 (1994).
4. Gray, M. W., Burger, G. & Lang, B. F. Mitochondrial evolution. *Science* **283,** 1476–1481 (1999).
5. Nakai, A. *et al.* The role of autophagy in cardiomyocytes in the basal state and in response to hemodynamic stress. *Nature Med.* **13,** 619–624 (2007).
6. Hemmi, H. *et al.* A Toll-like receptor recognizes bacterial DNA. *Nature* **408,** 740–745 (2000).
7. Taanman, J.-W. The mitochondrial genome: structure, transcription, translation and replication. *Biochim Biophys Acta Bioenerget.* **1410,** 103–123 (1999).
8. Collins, L., Hajizadeh, S., Holme, E., Jonsso, I. & Tarkowski, A. Endogenously oxidized mitochondrial DNA induces *in vivo* and *in vitro* inflammatory responses. *J. Leukoc. Biol.* **75,** 995–1000 (2004).
9. Mizushima, N., Levine, B., Cuervo, A. M. & Klionsky, D. J. Autophagy fights disease through cellular self-digestion. *Nature* **451,** 1069–1075 (2008).
10. Meerson, F., Zaletayeva, T., Lagutchev, S. & Pshennikova, M. Structure and mass of mitochondria in the process of compensatory hyperfunction and hypertrophy of the heart. *Exp. Cell Res.* **36,** 568–578 (1964).
11. Bugger, H. *et al.* Proteomic remodelling of mitochondrial oxidative pathways in pressure overload-induced heart failure. *Cardiovasc. Res.* **85,** 376–384 (2010).
12. Evans, C. J. & Aguilera, R. J. DNase II: genes, enzymes and function. *Gene* **322,** 1–15 (2003).
13. Kawane, K. *et al.* Chronic polyarthritis caused by mammalian DNA that escapes from degradation in macrophages. *Nature* **443,** 998–1002 (2006).
14. Ashley, N., Harris, D. & Poulton, J. Detection of mitochondrial DNA depletion in living human cells using PicoGreen staining. *Exp. Cell Res.* **303,** 432–446 (2005).
15. Kabeya, Y. *et al.* LC3, a mammalian homologue of yeast Apg8p, is localized in autophagosome membranes after processing. *EMBO J.* **19,** 5720–5728 (2000).
16. Yamaguchi, O. *et al.* Cardiac-specific disruption of the *c-raf-1* gene induces cardiac dysfunction and apoptosis. *J. Clin. Invest.* **114,** 937–943 (2004).
17. Lentz, S. I. *et al.* Mitochondrial DNA (mtDNA) biogenesis: visualization and duel incorporation of BrdU and EdU into newly synthesized mtDNA *in vitro*. *J. Histochem. Cytochem.* **58,** 207–218 (2010).
18. Takeuchi, O. & Akira, S. Pattern recognition receptors and inflammation. *Cell* **140,** 805–820 (2010).
19. Zhang, Q. *et al.* Circulating mitochondrial DAMPs cause inflammatory responses to injury. *Nature* **464,** 104–107 (2010).
20. Stunz, L. *et al.* Inhibitory oligonucleotides specifically block effects of stimulatory CpG oligonucleotides in B cells. *Eur. J. Immunol.* **32,** 1212–1222 (2002).
21. Bianchi, M. E. DAMPs, PAMPs and alarmins: all we need to know about danger. *J. Leukoc. Biol.* **81,** 1–5 (2007).
22. Nakahira, K. *et al.* Autophagy proteins regulate innate immune responses by inhibiting the release of mitochondrial DNA mediated by the NALP3 inflammasome. *Nature Immunol.* **12,** 222–230 (2011).
23. Yamaguchi, O. *et al.* Targeted deletion of apoptosis signal-regulating kinase 1 attenuates left ventricular remodeling. *Proc. Natl Acad. Sci. USA* **100,** 15883–15888 (2003).
24. Koizumi, T. Deoxyribonuclease II (DNase II) activity in mouse tissues and body fluids. *Exp. Anim.* **44,** 169–171 (1995).
25. Lu, Z. *et al.* Participation of autophagy in the degeneration process of rat hepatocytes after transplantation following prolonged cold preservation. *Arch. Histol. Cytol.* **68,** 71–80 (2005).
26. Mosgoller, W. *et al.* Distribution of DNA in human Sertoli cell nucleoli. *J. Histochem. Cytochem.* **41,** 1487–1493 (1993).

Supplementary Information is linked to the online version of the paper at www.nature.com/nature.

Acknowledgements We thank S. Nagata and K. Kawane, Kyoto University, for discussions and a gift of *Dnase2a*$^{flox/flox}$ mice, and Y. Uchiyama, Juntendo University, for anti-LC3 antibody. We also thank K. Takada for technical assistance. This work was supported by a Grant-in-Aid for Scientific Research from the Ministry of Education, Culture, Sports, Science and Technology in Japan and research grants from Mitsubishi Pharma Research Foundation and the British Heart Foundation (CH/11/3/29051, RG/11/12/29052).

Author Contributions S.A. and I.K. provided intellectual input; K.O. was responsible for the overall study design and writing the manuscript. The other authors performed experiments and analysed data. All authors contributed to the discussions.

Author Information Reprints and permissions information is available at www.nature.com/reprints. The authors declare no competing financial interests. Readers are welcome to comment on the online version of this article at www.nature.com/nature. Correspondence and requests for materials should be addressed to K.O. (kinya.otsu@kcl.ac.uk).

METHODS

Animal study. The study was performed under the supervision of the Animal Research Committee of Osaka University and in accordance with the Japanese Act on Welfare and Management of Animals (No. 105).

We crossed mice bearing a *Dnase2a*^{flox} allele[13] with transgenic mice expressing *Cre* recombinase under the control of the α-myosin heavy chain promoter (α-MyHC)[16], to produce cardiac-specific DNase II-deficient mice, *Dnase2a*$^{flox/flox}$;α-MyHC-*Cre*$^{+}$ (*Dnase2a*$^{-/-}$). To generate double-knockout mice of *Dnase2a* and *Tlr9*, we crossed *Dnase2a*$^{-/-}$ mice with *Tlr9*$^{-/-}$ mice[6].

The 12- to 14-week-old male mice were subjected to TAC[5,23] and severe TAC using 26- and 27-gauge needles for aortic constriction, respectively. Non-invasive measurements of blood pressure were performed on mice anaesthetized with 2.5% avertin using a blood pressure monitor for rats and mice Model MK-2000 (Muromachi Kikai) according to the manufacturer's instructions[5,23]. To perform echocardiography on awakened mice, ultrasonography (SONOS-5500, equipped with a 15 MHz linear transducer, Philips Medical Systems) was used. The heart was imaged in the two-dimensional parasternal short-axis view, and an M-mode echocardiogram of the midventricle was recorded at the level of the papillary muscles. Heart rate, intraventricular septum and posterior wall thickness, and end-diastolic and end-systolic internal dimensions of the left ventricle were obtained from the M-mode image.

Measurement of DNase II activity. The DNase II activity was determined using the single radial enzyme-diffusion method[24]. The heart homogenates were applied to the cylindrical wells (radius, 1.5 mm) punched in 1% (w/v) agarose gel, containing 0.05 mg ml^{-1} salmon sperm DNA (Type III), 5 μg ml^{-1} ethidium bromide, 0.5 M sodium acetate buffer (pH 4.7) and 10 mM EDTA. After incubation for 48 h at 37 °C, the radius of the dark circle was measured under an ultraviolet transilluminator at 312 nm. DNase II activities for the samples were determined using a standard curve constructed from the serial dilution of porcine DNase II (Sigma).

Quantitative RT–PCR. Total RNA was isolated from the left ventricle or cultured cardiomyocytes for analysis using the TRIzol reagent (Invitrogen Life Technologies). The mRNA levels were determined by quantitative RT–PCR[5]. For reverse transcription and amplification, we used the TaqMan Reverse Transcription Reagents (Applied Biosystems) and Platinum Quantitative PCR SuperMix-UDG (Invitrogen Life Technologies), respectively. The PCR primers and probes were obtained from Applied Biosystems. The primers used were as follows: *Nppa* assay identity, mm01255747_g1; *Nppb* assay identity, mm00435304_g1; *Col1a2* assay identity, Mm01165187_m1; *Gapdh* assay identity, 4352339E; *Il6* assay identity, Mm99999064_m1; *Il1b* assay identity, Mm01336189_m1; *Ifnb1* assay identity, Mm00439546_s1; *Ifng* assay identity, Mm99999071_m1; *Tnf* assay identity, Mm00443260_g1; and *Dnase2a* assay identity, Mm00438463_m1. We constructed quantitative PCR standard curves using the corresponding complementary DNA, and all data were normalized to *Gapdh* mRNA content.

Histological analysis. Heart samples were excised and immediately fixed in buffered 4% paraformaldehyde, embedded in paraffin and cut into 5 μm sections. Haematoxylin and eosin or AZAN-Mallory staining was performed on serial sections[5,23]. Myocyte cross-sectional area was measured by tracing the outline of 100–200 myocytes in each section[5,23]. For immunohistochemical analysis, frozen heart sections (5 μm) were fixed in buffered 4% paraformaldehyde. The antibodies used were anti-mouse CD45 (ANASPEC), CD68 (Serotec), Ly6G/6C (BD Pharmingen), CD3 (Abcam), LAMP2a (Zymed), LC3 (ref. 25) and TLR9 (Santa-Cruz). For *in situ* hybridization analysis, the mouse IL-6 (1-636) and IL-1β (1-810) RNA probes were labelled using a DIG RNA Labelling Kit and detected using a DIG Nucleic Acid Detection Kit (Roche Diagnostics). For immunoelectron microscopy, frozen heart tissue was embedded in LR White resin and the deposited DNA was detected using anti-DNA antibody (Abcam) and immunogold conjugated anti-mouse IgG (British Biocell International)[26]. For DNA detection, heart sections were incubated in PicoGreen (Molecular Probes) for 1 h. We used EdU to detect mitochondrial DNA in the heart section. Twenty-four hours before TAC, mice were injected intraperitoneally with 250 μg of EdU every 2 h five times, and EdU was detected using a Click-iT EdU Alexa Fluor 488 Imaging Kit (Invitrogen).

***In vitro and in vivo* rescue experiments with the TLR9 inhibitor.** Adult mouse cardiomyocytes were isolated from 12- to 14-week-old male mouse hearts as we previously described[5]. Cardiomyocytes were pre-treated with 1 μg ml^{-1} inhibitory CpG oligodeoxynucleotides (ODN2088) (Operon) (5′-TCCTGGCGGGGAA GT-3′) or control oligodeoxynucleotides (ODN2088 control) (5′-TCCTGAGC TTGAAGT-3′) for 5 h and incubated with 20 nM CCCP or 50 μM isoproterenol for 24 h (ref. 20). Cell death was estimated by Trypan blue staining[5]. To monitor mitochondrial membrane potential ($\Delta\psi$), the cells were loaded with tetramethylrhodamine ethyl ester (Molecular Probes) at 10 nM for 30 min before observation. In *in vivo* study, the mice were injected intravenously with 500 μg of the oligodeoxynucleotides 2 h before and 2 days after TAC, and they were analysed 4 days after TAC. To estimate survival, the mice received additional administration of the oligodeoxynucleotides 4 days after TAC and every 3 days thereafter.

Statistical analysis. Results are shown as the mean ± s.e.m. Paired data were evaluated using a Student's *t*-test. A one-way analysis of variance with the Bonferroni post hoc test was used for multiple comparisons. The Kaplan–Meier method with a log-rank test was used for survival analysis.

CORRIGENDUM

doi:10.1038/nature11515

Corrigendum: Mitochondrial DNA that escapes from autophagy causes inflammation and heart failure

Takafumi Oka, Shungo Hikoso, Osamu Yamaguchi, Manabu Taneike, Toshihiro Takeda, Takahito Tamai, Jota Oyabu, Tomokazu Murakawa, Hiroyuki Nakayama, Kazuhiko Nishida, Shizuo Akira, Akitsugu Yamamoto, Issei Komuro & Kinya Otsu

Nature **485,** 251–255 (2012); doi:10.1038/nature10992

In this Letter, several images were mistakenly switched or duplicated during preparation of the artwork. In Figs 1f and 2a, the sham-operated *Dnase2a*$^{-/-}$ and TAC-operated *Dnase2a*$^{+/+}$ mice panels were switched. In Fig. 4d, the panel showing CD3 staining for ODN2088 control-treated TAC-operated *Dnase2a*$^{+/+}$ mice (now shown correctly as black-bordered panel in Fig. 1 below) is a duplicate of that showing Ly6G staining for ODN2088-treated TAC-operated *Dnase2a*$^{-/-}$ mice. The panel showing CD45 staining for ODN2088-treated TAC-operated *Dnase2a*$^{+/+}$ (now shown correctly as blue-bordered panel in Fig. 1 below) was prepared from the original picture of ODN2088 control-treated TAC-operated *Dnase2a*$^{+/+}$. In Supplementary Fig. 4c, sham-operated *Dnase2a*$^{-/-}$ and TAC-operated *Dnase2a*$^{+/+}$ mice panels were switched. Finally, in Supplementary Fig. 10d, the panels showing CD3 and Ly6G staining for sham-operated *Tlr9*$^{+/+}$ mice were switched. These corrections do not alter any of the conclusions of this Letter, and the authors apologize for any confusion these errors may have caused.

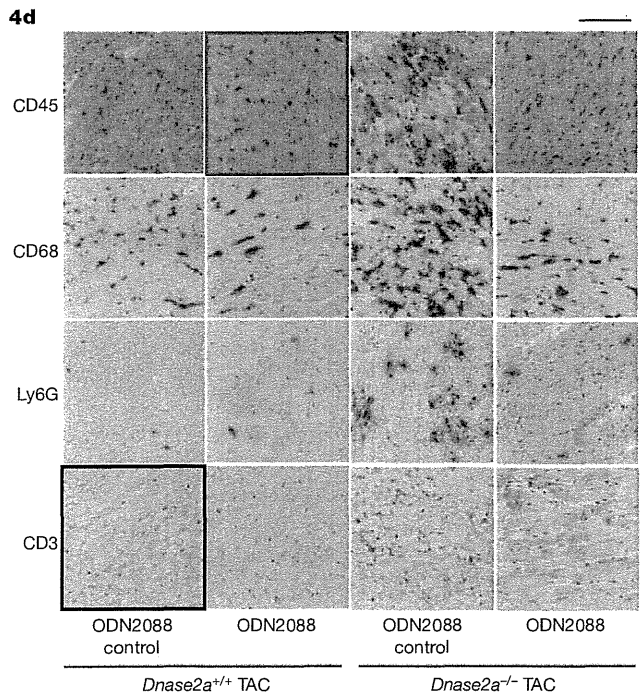

Figure 1 | This is the corrected Fig. 4d of the original Letter.

Circulation Journal
Official Journal of the Japanese Circulation Society
http://www.j-circ.or.jp

Impact of Preoperative Percutaneous Cardiopulmonary Support on Outcome Following Left Ventricular Assist Device Implantation

Koichi Toda, MD, PhD; Tomoyuki Fujita, MD; Junjiro Kobayashi, MD, PhD; Yusuke Shimahara, MD; Soichiro Kitamura, MD, PhD; Osamu Seguchi, MD, PhD; Yoshihiro Murata, MD; Masanobu Yanase, MD; Takeshi Nakatani, MD, PhD

Background: The purpose of the present study was to determine the impact of preoperative percutaneous cardiopulmonary support (PCPS) on long-term survival following implantation of a left ventricular assist device (LVAD).

Methods and Results: Between 1999 and 2010, we used implantable (n=12) and paracorporeal (n=91) LVADs in 103 consecutive cardiomyopathy patients as a bridge to transplantation. Prior to LVAD implantation, all patients received inotropes, and 25 patients (24%) received PCPS because of cardiogenic shock. Postoperatively, there were no early mortalities within 30 days after surgery, and patients survived on LVAD for 560±391 days, of whom 9 patients recovered and 32 underwent heart transplantation after 711±360 days of LVAD support. More patients with preoperative PCPS required nitric oxide inhalation and prolonged inotropic support to maintain adequate LVAD flow. In addition, bilirubin level at 1 month after LVAD implantation was significantly higher in patients with preoperative PCPS. Cox regression analysis identified preoperative PCPS support as the only significant predictor for death after LVAD implantation and overall survival was significantly better in patients without preoperative PCPS.

Conclusions: Despite adequate hemodynamic support after LVAD implantation, patients with preoperative PCPS had significantly worse survival. LVAD should be used for patients with end-stage heart failure, before PCPS is required for hemodynamic support. (*Circ J* 2012; **76:** 88–95)

Key Words: Cardiomyopathy; Heart-assist devices; Heart failure; Surgery; Transplantation

Mechanical circulatory support with a left ventricular assist device (LVAD) has become a well-established procedure for patients with end-stage heart failure. Patient selection and timing of implantation, however, remain critical issues. Although several studies have identified pre-implantation risk factors in regard to mortality,[1,2] most are limited by the fact that few of the reported patients were supported by an LVAD for a prolonged period. Because prolonged LVAD support has become prevalent not only as a bridge to transplantation but also for destination therapy, it is important to find preoperative risk factors for patients supported by an LVAD for a prolonged period. Preoperative cardiogenic shock is recognized as one of the significant risk factors for mortality after LVAD implantation,[2,3] and percutaneous cardiopulmonary support (PCPS), has been utilized for patients in cardiogenic shock to improve and stabilize the preoperative condition of LVAD candidates.[4,5] Although those studies demonstrated that PCPS can effectively act as a bridge to LVAD therapy for patients in cardiogenic shock, the duration of LVAD support in previous studies was relatively short, and the impact of preoperative PCPS on long-term LVAD support is not known. In Japan, because of a severe donor shortage, the average LVAD support period before heart transplantation is >2 years,[6] which provides a unique opportunity to observe LVAD patients for prolonged periods. In the present study we retrospectively reviewed 103 consecutive patients to clarify the impact of preoperative PCPS on long-term survival following implantation of an LVAD.

Methods

Patients

This study was conducted as a retrospective analysis of 103 consecutive cardiomyopathy patients who underwent LVAD implantation as a bridge to heart transplantation at National Cerebral and Cardiovascular Center, Osaka, between May

Received March 28, 2011; revised manuscript received August 21, 2011; accepted September 14, 2011; released online December 3, 2011 Time for primary review: 60 days

Department of Cardiovascular Surgery (K.T., T.F., J.K., Y.S., S.K.), Department of Transplantation (O.S., Y.M., M.Y., T.N.), National Cerebral and Cardiovascular Center, Suita, Japan

Mailing address: Koichi Toda, MD, PhD, Department of Cardiovascular Surgery, National Cerebral and Cardiovascular Center, 5-7-1 Fujishiro-dai, Suita 565-8565, Japan. E-mail: ktoda2002@yahoo.co.jp

ISSN-1346-9843 doi:10.1253/circj.CJ-11-0339

Table 1. Preoperative Patient Characteristics	
Gender (M/F)	73 (71)/30 (29)
Age (years)	34±13
BSA (m^2)	1.56±0.20
BMI (kg/m^2)	19.1±3.6
Duration of heart failure (months)	54±59
Serum total bilirubin (mg/dl)	2.3±2.1
Serum creatinine (mg/dl)	1.5±1.2
Serum BNP (pg/ml)	1,484±1,066
Preoperative IABP support	42 (41)
Preoperative PCPS	25 (24)
Previous cardiac surgery	14 (14)
LVEDD (mm)	74±11
LVESD (mm)	68±12
LAD (mm)	47±9
LVEF (%)	17±8
Cardiac index ($L \cdot min^{-1} \cdot m^{-2}$)	1.9±0.6

Data given as mean±SD or n (%).
BSA, body surface area; BMI, body mass index; BNP, brain natriuretic peptides; PCPS, percutaneous cardiopulmonary support; LVEDD, left ventricular end-diastolic diameter; LVESD, left ventricular end-systolic diameter; LVEF, left ventricular ejection fraction.

1999 and July 2010. All patients had been hospitalized at least once for New York Heart Association class IV heart failure and were receiving maximized medical regimens, including angiotensin-converting enzyme inhibitors, beta-blockers, and diuretics. Histological diagnosis was made based on preoperative biopsy findings, while the etiology of cardiomyopathy included dilated cardiomyopathy (n=73), dilated phase of hypertrophic cardiomyopathy (n=12), and secondary cardiomyopathy (myopathy, n=7; ischemia, n=6; sarcoidosis, n=3; drug, n=2). Prior to LVAD implantation, all patients were receiving i.v. inotropes. Furthermore 42 (41%) were supported by IABP alone, and 25 (24%) by PCPS, which consisted of a membrane oxygenator and centrifugal pump (Capiox, Terumo, Tokyo, Japan). Of 25 patients who were initially supported by PCPS before LVAD implantation, 12 required PCPS in order to improve multi-organ failure due to acute deterioration of heart failure; 6 required PCPS because of sudden hemodynamic collapse due to ventricular arrhythmia or cardiac arrest; 5 required PCPS because of acute hemodynamic collapse due to sepsis; 1 required PCPS during high-risk percutaneous coronary intervention for acute myocardial infarction and could not be weaned from it; and 1 could not be weaned from PCPS after high-risk coronary artery bypass grafting (CABG) with a mitral annuloplasty. Baseline characteristics are presented in Table 1. As indicators of preoperative multi-organ failure, serum creatinine was >2.0 mg/dl in 16 patients (16%), and total bilirubin was >2.0 mg/dl in 45 patients (44%). Fourteen patients (14%) had a history of previous cardiac surgery including restrictive mitral annuloplasty (n=4), partial left ventriculectomy with mitral surgery (n=3), mitral valve replacement (n=2), surgical ventricular reconstruction with CABG (n=2), CABG (n=2), and LVAD placement (n=1). Preoperative left ventricular (LV) and atrial dimension and function, and cardiac output were evaluated on echocardiography (Table 1). The institutional ethics committee of National Cerebral and Cardiovascular Center approved this study and written informed consent for the procedure was obtained from all patients before surgery.

Table 2. Operative Data	
Cardiopulmonary bypass time (min)	161±54
Aortic cross-clamp time (min)	53±30
Concomitant procedures	
Tricuspid annuloplasty	58 (56)
Restrictive mitral annuloplasty	6 (6)
Removal of left ventricular thrombus	3 (3)
Partial left ventriculectomy	2 (2)
Implantation of CRT leads	2 (2)
Closure of patent foramen ovale	2 (2)
Right ventricular mechanical support	2 (2)
Closure of ventricular septal defect	1 (1)
Coronary artery bypass grafting	1 (1)
Cryoablation for ventricular tachycardia	1 (1)

Data given as mean±SD or n (%).
CRT, cardiac resynchronization therapy.

Surgical Technique

All surgical procedures were performed through a median sternotomy under a cardiopulmonary bypass (CPB). The outflow cannula was anastomosed to the ascending aorta, and inflow to the LV apex, without arresting the heart, to minimize ischemic insult to the right ventricle. The LVAD was then placed between the inflow and outflow cannulae. Ninety-one paracorporeal devices (Toyobo-VAS: Nipro) and 12 implantable devices (3 HeartMate VE [Thoratec]; 4 Novacor [WorldHeart]; 3 EVAHEART [SUN MEDICAL], 1 Jarvik 2000 [Jarvik Heart]; and 1 HeartMate II [Thoratec]) were used as the LVADs. In addition, 78 concomitant procedures were performed and tepid blood cardioplegia was given in antegrade and retrograde fashion to obtain cardioplegic arrest in 9 cases.

Postoperative Management

During the immediate postoperative period pulmonary artery pressure and cardiac output were monitored, while cardiac output was maximized by optimizing the volume status and dosage of inotropes and phosphodiesterase inhibitor (PDEi). While the patient was intubated, nitric oxide was given in order to reduce pulmonary vascular resistance, and nitric oxide inhalation was switched to i.v. (Milrinone) and/or oral PDEi (Sildenafil) after extubation. After removing the pulmonary artery catheter, cardiac output was estimated, and volume status and right ventricular function were evaluated on transthoracic echocardiography. Echocardiographic measurement included LV end-diastolic and end-systolic diameters, left atrial diameter, LV ejection fraction and other routine variables, and cardiac output was measured at the right ventricular outflow tract. Anticoagulation was started using i.v. low-molecular-weight heparin within 24 h after surgery, then switched to coumadin to maintain an international normalized ratio between 3 and 4 for patients with a Toyobo-VAS, or between 2 and 3 for patients with implantable devices (except for the HeartMate VE: only aspirin was given to these patients). After patients were discharged from the intensive care unit (ICU), ambulation was encouraged and cardiac rehabilitation was commenced. Those with an implantable device were discharged to home, after being trained to care for themselves and their device.

Statistical Analysis

Preoperative and postoperative variables were investigated by reviewing clinical records. Continuous variables are expressed as mean±SD and were compared using a Mann–Whitney

Table 3. Predictors of Death After LVAD Implantation: Cox Proportional Hazards Analysis

	Hazard ratio	P value
Female	1.22	0.5431
Age >50 years	1.66	0.1986
BMI ≤20 kg/m²	0.80	0.498
Duration of heart failure ≥5 years	1.17	0.195
Dilated cardiomyopathy	0.78	0.5817
Previous cardiac surgery	1.83	0.1257
Creatinine ≥2 mg/dl	1.49	0.3149
Total bilirubin ≥2 mg/dl	1.45	0.2382
LVEF ≤20%	0.76	0.4029
LVEDD ≥75 mm	0.94	0.8538
Paracorporeal LVAD	2.00	0.2491
Preoperative PCPS	2.23	0.0178
Preoperative IABP	0.59	0.1125

LVAD, left ventricular assist device. Other abbreviations see in Table 1.

U-test for unpaired data and a Wilcoxon signed rank test for paired data. Categorical variables were compared using Fisher's exact test. Predictors of death were analyzed using a Cox proportional hazards model. Actuarial survival was analyzed using the Kaplan–Meier method, and survival curves were compared using a log-rank test. Data were analyzed using StatView 5.0 (SAS Institute, Cary, NC, USA) and $P<0.05$ was considered to be statistically significant.

Results

Early Results

We performed 78 concomitant procedures at the time of LVAD implantation and the mean CPB time was 161±54 min. Cardioplegic arrest was avoided as much as possible to reduce ischemic insult to the right ventricle. Cardioplegic arrest was applied in 9 patients and aortic cross-clamp time was 53±30 min (Table 2). Thirty-seven patients (36%) were weaned from CPB with nitric oxide inhalation and 2 patients who had PCPS preoperatively required mechanical right ventricular support for weaning from CPB. With regard to those 2 patients, right ventricular function was recovered and mechanical right ventricular support was removed at 8 days after LVAD implantation in 1 patient, while long-term right ventricular support with a Toyobo-VAS was required in the other. In addition, 23 patients (22%) required re-exploration for mediastinal bleeding and 18 (17%) required a tracheostomy for prolonged respiratory support. Although 16 patients (16%) required continuous hemofiltration to treat postoperative acute renal failure, none needed chronic hemodialysis and there were no early mortalities within 30 days after LVAD implantation among the 103 LVAD patients.

Late Results

The patients had an LVAD for 560±391 days (range, 17–1,567 days). During LVAD support 48 patients had 113 cerebrovascular events including hemorrhage, infarction, and transient ischemic attacks, and the rate of cerebrovascular events was calculated to be 0.72 events per patient per year. Bloodstream infections occurred in 57 patients (55%), from whom the LVAD was removed in 2 and exchanged in 1 because of an intractable bloodstream infection. When right ventricular fail-

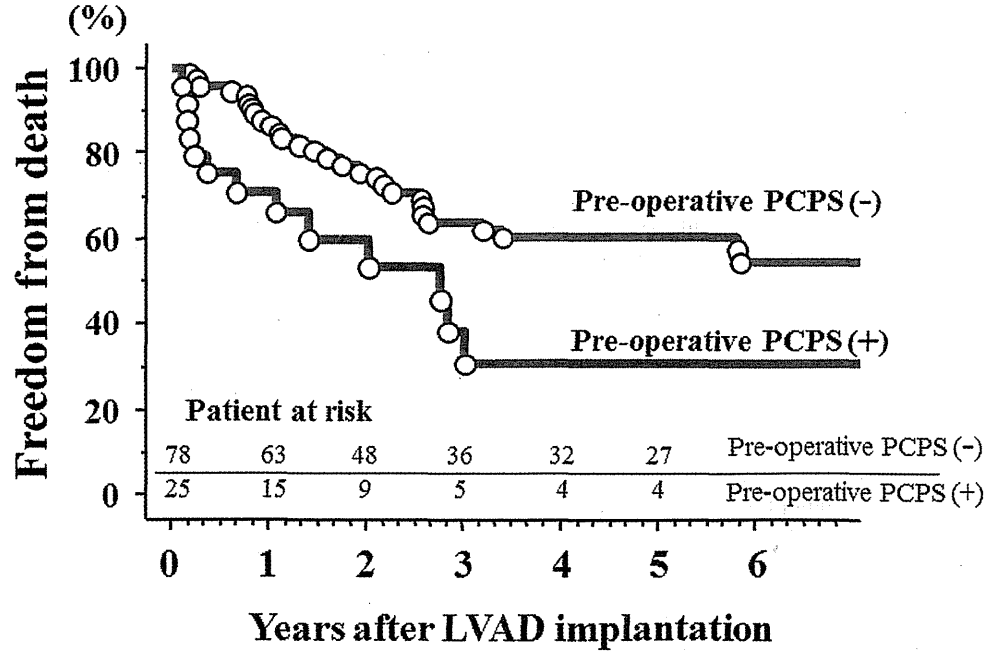

Figure 1. Survival after left ventricular assist device (LVAD) implantation as a bridge to transplantation in 103 cardiomyopathy patients. Red, patients with preoperative percutaneous cardiopulmonary support (PCPS); blue, patients without preoperative PCPS. There was a significant difference in survival between the groups (P=0.015; log-rank test).

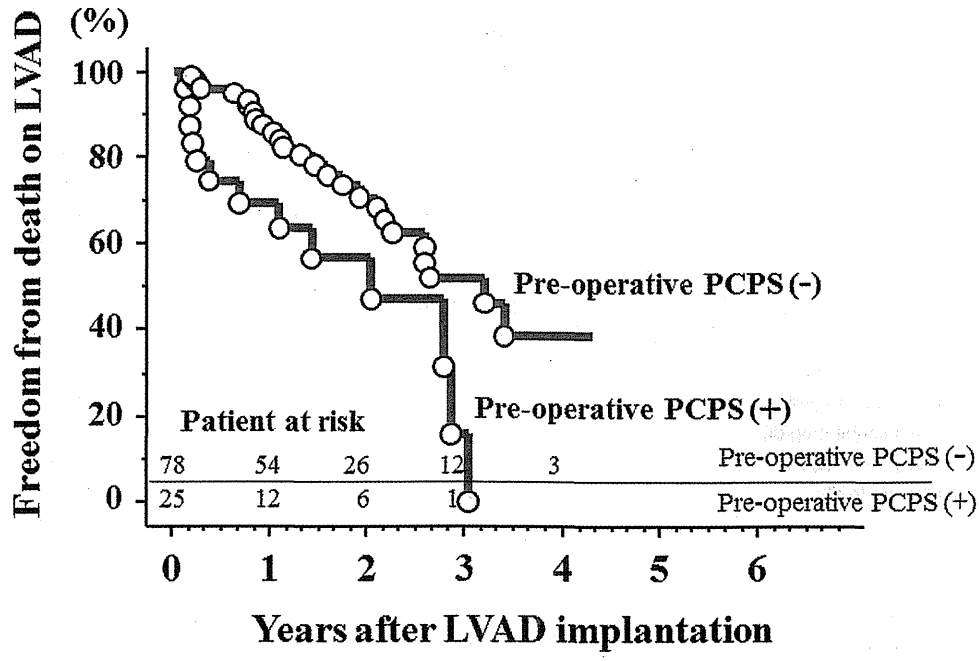

Figure 2. Survival while on left ventricular assist device (LVAD) support in patients (red) with and (blue) without preoperative percutaneous cardiopulmonary support (PCPS). There was a significant difference in survival between the groups (P=0.0052; log-rank test).

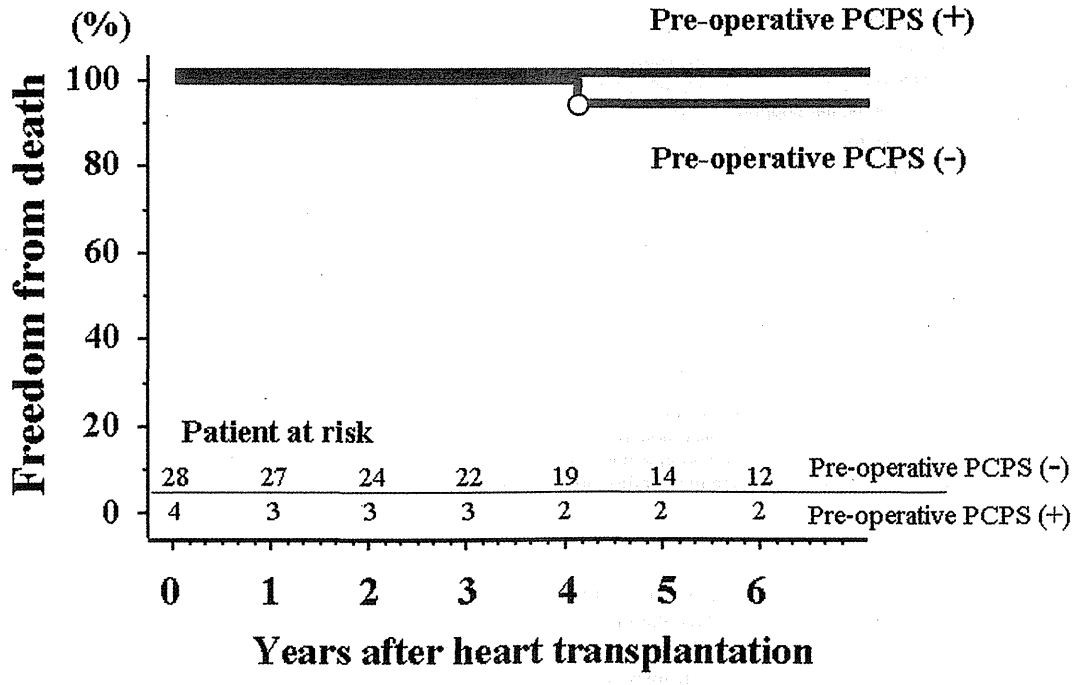

Figure 3. Kaplan–Meier survival curve after heart transplantation in 32 cardiomyopathy patients who underwent left ventricular assist device (LVAD) implantation as a bridge to transplantation. Red, patients with preoperative percutaneous cardiopulmonary support (PCPS); blue, patients without preoperative PCPS.

Table 4. Preoperative Variables vs. Preoperative PCPS

	PCPS (–)	PCPS (+)	P value
Female gender	23/78 (29)	7/25 (28)	>0.999
Dilated cardiomyopathy	59/78 (75)	14/25 (56)	0.0776
IABP support	42/78 (54)	22/25 (88)	0.0020
Mechanical ventilation	6/78 (8)	22/25 (88)	<0.0001
Age (years)	35±13	33±12	0.4347
BSA (m^2)	1.56±0.21	1.55±0.16	0.9216
BMI (kg/m^2)	19.1±3.8	19.0±2.6	0.7263
Duration of heart failure (months)	57±58	45±64	0.0431
White blood cell count (/ml)	8,652±2,992	10,967±4,861	0.0453
Hemoglobin (g/dl)	11.2±2.0	10.0±1.7	0.0056
Platelet count ($\times 10^4$/ml)	23.3±19.0	13.0±7.9	<0.0001
C-reactive protein (mg/dl)	3.6±3.5	6.4±4.8	0.0127
Serum total bilirubin (mg/dl)	1.9±1.2	3.4±3.5	0.0126
Serum total protein (g/dl)	6.4±0.6	6.0±0.7	0.0071
Serum albumin (g/dl)	3.6±0.4	3.2±0.7	0.029
AST (IU/L)	133±331	247±528	0.099
ALT (IU/L)	173±388	219±412	0.3482
Serum creatinine (mg/dl)	1.3±0.9	2.0±1.8	0.2427
Serum BUN (mg/dl)	32±22	42±27	0.0818
Serum sodium (mmol/L)	130±7	137±9	0.0004
Serum BNP (pg/ml)	1,516±1,048	1,394±1,093	0.5352

Data given as mean±SD or n (%).
AST, aspartate aminotransferase; ALT, alanine aminotransferase; BUN, blood urea nitrogen. Other abbreviations see in Tables 1,2.

Table 5. Early Postoperative Outcome at 1-Month After LVAD Implantation vs. Preoperative PCPS

	PCPS (–)	PCPS (+)	P value
Nitric oxide inhalation	22/78 (28)	15/25 (60)	0.0098
Acute renal failure	7/78 (9)	9/25 (36)	0.004
Prolonged ventilation	6/78 (8)	12/25 (48)	<0.0001
Mechanical right ventricular support	0/78 (0)	2/25 (8)	0.0571
Right ventricular failure	12/78 (15)	9/25 (36)	0.0431
Total bilirubin (mg/dl)	1.6±2.3	3.4±5.8	0.0276
Creatinine (mg/dl)	0.7±0.4	0.7±0.5	0.6021
LVEDD (mm)	59±18	62±16	0.5701
LVESD (mm)	53±19	53±19	0.9995
LAD (mm)	31±9	33±7	0.5458
LVEF (mm)	23±17	28±17	0.2630
Cardiac index ($L \cdot min^{-1} \cdot m^{-2}$)	3.5±0.9	3.8±0.8	0.2135

Data given as mean±SD or n (%).
Nitric oxide inhalation, nitric oxide inhalation for weaning from cardiopulmonary bypass; acute renal failure, acute renal failure requiring continuous hemofiltration; prolonged ventilation, mechanical ventilation >2-weeks; right ventricular failure, right ventricular failure requiring a right ventricular assist device or ≥30-days of inotropic support after LVAD implantation; LAD, left atrial diameter; cardiac index, estimated on echocardiogram. Other abbreviations see in Tables 1,2.

ure was defined as requiring mechanical right ventricular support or ≥30 days of inotropic support after LVAD implantation, 21 patients (20%) developed right ventricular failure.

Of the 103 patients studied, 32 underwent heart transplantation after 711±360 days (range, 99–1,444 days) of LVAD support and 1 patient died of infection at 4 years after transplantation. Furthermore, 25 patients remained on LVAD support at the time of writing, while 9 (9%) recovered and the LVAD was explanted. In contrast, 37 patients died during LVAD support. The major causes of death in those cases were cerebrovascular events in 18 patients, sepsis in 15, and right ventricular failure in 4.

Predictors of Survival After LVAD Implantation

With a mean follow-up period of 1,274±1,174 days (range, 34–4,102 days), the overall survival rate was 84% at 1 year, 72% at 2 years, and 59% at 3 years after LVAD implantation. Univariate analysis with a Cox proportional hazards model showed that preoperative PCPS was the only significant predictor for death after LVAD implantation (hazard ratio, 2.23, P=0.0178; 95% confidence interval, 1.15–4.31; Table 3). Kaplan–Meier curve demonstrated that survival at 3 years

after LVAD implantation was 38% in patients with preoperative PCPS and 64% in those without, while log-rank analysis indicated significantly better survival in patients without preoperative PCPS (**Figure 1**). Kaplan–Meier analysis was also used to characterize survival while on LVAD support, in which LVAD explantation or heart transplantation, and the end of the observation period were regarded as censoring events. This showed that survival during LVAD support was significantly better in patients without preoperative PCPS (**Figure 2**). We also analyzed survival after heart transplantation using Kaplan–Meier curves, which demonstrated that survival after heart transplantation in patients with preoperative PCPS was as good as that of patients without preoperative PCPS (**Figure 3**).

Preoperative Variables and Early Postoperative LVAD Outcomes vs. Preoperative PCPS

Preoperative variables (**Table 4**) and early postoperative outcomes including postoperative complications, end-organ functions, and echocardiographic data obtained at 1 month after LVAD implantation (**Table 5**) were compared between patients with and without preoperative PCPS. Preoperatively a greater number of patients with PCPS required IABP support and mechanical ventilation. White blood cell count, and serum total bilirubin and C-reactive protein levels before LVAD implantation were significantly higher in the patients with preoperative PCPS, while hemoglobin, platelet count, and serum total protein, albumin, and sodium levels before LVAD implantation were significantly lower in those with preoperative PCPS (**Table 4**).

Those with preoperative PCPS required nitric oxide inhalation more frequently in order to be weaned from CPB at the time of operation, and continuous hemofiltration more frequently for postoperative acute renal failure, while a greater number of patients with preoperative PCPS required prolonged mechanical ventilation for >2 weeks after LVAD implantation. At 1 month after LVAD implantation, serum total bilirubin remained significantly higher in patients with preoperative PCPS as compared to those without, and more patients with preoperative PCPS required inotropic support to maintain an adequate LVAD pump flow. In contrast, echocardiography indicated similarly reduced LV and atrial diameters, as well as adequate cardiac output in both groups (**Table 5**).

Discussion

The major finding of the present study is that patients who required PCPS for preoperative cardiogenic shock had a significantly worse rate of survival during long-term LVAD support as compared to those who did not require preoperative PCPS. This result is consistent with findings presented by The Interagency Registry for Mechanically Assisted Circulatory Support (INTERMACS), which found that the INTERMACS Level 1 category, characterized by cardiogenic shock with life-threatening hypoperfusion, is one of the risk factors for death after LVAD implantation.[2] In the present series, mean arterial pressure was maintained at 71±16 mmHg and serum lactate level was also stabilized at 1.6±1.1 mmol/L during PCPS (normal <2.0 mmol/L). All but 1 recovered from anuria or oliguria and their urine output was maintained at 662±349 ml for the last 6 h before LVAD implantation, and serum creatine level improved from 3.4±2.0 mg/dl to 1.6±1.3 mg/dl during PCPS (P=0.0173). Although they were considered to be hemodynamically stabilized by PCPS at the time of LVAD implantation, those patients still had a significantly worse prognosis after LVAD implantation as compared with patients without preoperative PCPS. This result may emphasize the importance of timing of LVAD implantation, because it indicates that it is difficult to recover from damage caused by acute deterioration of heart failure and have an improved prognosis once acute deterioration of heart failure develops.

As compared to the INTERMACS data, the present study is unique because of the prolonged duration of LVAD support (mean, 560±391 days; range, 17–1,567 days) in the present subjects. Prolonged LVAD support has become more important not only as a bridge to transplantation but also as destination therapy. Although preoperative risk factors were analyzed in patients who underwent LVAD implantation as a destination therapy, the endpoint of the study was 90-day in-hospital mortality and the impact of preoperative factors on late mortality during long-term LVAD support remains to be elucidated.[7] The overall survival rates in the present series were 84% at 1 year and 72% at 2 years, and similarly excellent long-term LVAD support have been reported from Japan,[3,8] where the average LVAD support period before heart transplantation is >2 years. As a result, the Japanese Registry for Mechanically Assisted Circulatory Support (J-MACS registry), which was recently started, may facilitate identification of preoperative risk factors for long-term LVAD support in a future study.

Although there were no deaths within 30 days after LVAD implantation, early postoperative complications were more frequent in patients with preoperative PCPS, who required prolonged mechanical ventilation and continuous hemofiltration. At 1 month after LVAD implantation total bilirubin level was significantly higher in patients with preoperative PCPS, although the dilated LV and atrial diameters were reduced and adequate cardiac output was maintained similarly in both groups (**Table 5**). This may indicate that patients with preoperative PCPS did not recover from preoperative end-organ dysfunction due to cardiogenic shock at 1 month after LVAD implantation, despite cardiac output being adequately maintained. Masai et al reported that a group of LVAD patients who died from multi-organ failure despite adequate hemodynamic support had increased levels of interleukin (IL)-6 and IL-8.[9] In addition, other studies have suggested that ongoing systemic inflammatory response syndrome (SIRS) plays a key role in the development of multi-organ failure in patients who die from multi-organ failure despite adequate hemodynamic support.[10] In the present series, preoperative white blood cell count and serum C-reactive protein level were significantly higher in patients with PCPS, which suggests that preoperative SIRS induced by PCPS[11] may have a harmful impact on end-organ dysfunction after LVAD implantation.

PCPS is a well-established extracorporeal life support system that can be set up quickly without a thoracotomy and provides emergency circulatory assistance for cardiogenic shock,[12] and it can be used as a bridge to a long-term mechanical circulatory support device.[4,5] The impact of preoperative PCPS on LVAD support, however, remains inconclusive. McCarthy et al found that prior PCPS was a significant risk factor for death after LVAD implantation,[13] whereas Pagani et al reported that preoperative PCPS was not a risk factor for death after LVAD implantation.[4,5] When we compared overall survival after LVAD implantation (**Figure 1**) and survival on LVAD (**Figure 2**), patients with preoperative PCPS had significantly worse survival in both analyses and the level of statistical significance was even greater for survival on LVAD (P=0.015, **Figure 1** vs. P=0.0052, **Figure 2**). This suggests that the prognosis of preoperative PCPS patients was much worse while on LVAD. In contrast, survival after heart trans-

plantation was good in LVAD-supported patients irrespective of pre-LVAD PCPS (**Figure 3**), which shows that pre-LVAD PCPS may not lead to worse survival if the waiting time before heart transplantation, which is currently as long as 2 years in Japan because of donor shortage, could be reduced.

The incidence of right ventricular failure after LVAD implantation was higher in patients with preoperative PCPS,[5] and preoperative circulatory support was the most significant risk factor for mechanical right ventricular support after LVAD implantation.[14] In the present series, more patients with preoperative PCPS developed right ventricular failure, which required prolonged i.v. inotropic support after LVAD implantation. This increased incidence of right ventricular failure in patients with preoperative PCPS may be attributable in part to lung injury exacerbated by preoperative PCPS,[11] in addition to pre-existing right ventricular dysfunction, which is unmasked with the increase in right-sided preload afforded by LVAD support.[15] This speculation is supported by the fact that more patients with preoperative PCPS required nitric oxide inhalation for reduction of pulmonary vascular resistance in order to be weaned from CPB. Further studies are necessary to clarify to what extent preoperative PCPS itself affects right ventricular function by inducing lung injury.

We utilized right ventricular mechanical support in 2 patients who required preoperative PCPS, while such support was not required in any patients without preoperative PCPS. Kirsch et al were more aggressive in utilizing mechanical right ventricular support in patients who underwent LVAD implantation, and 79% of their patients received mechanical right ventricular support.[16] As shown in **Table 5**, patients who required preoperative PCPS developed right ventricular failure more frequently (36% vs. 15%, P=0.0431) and their total bilirubin level was higher (3.4±5.8 mg/dl vs. 1.6±2.3 mg/dl, P=0.0276) at 1 month after LVAD implantation as compared with patients without preoperative PCPS. These results indicate that some patients who initially required PCPS developed right ventricular failure and hepatic failure after LVAD implantation, which may have been the reasons for the worse survival in patients with preoperative PCPS. When we compared the incidence of postoperative right ventricular dysfunction requiring inotropic support and total bilirubin level between patients who died within 100 days after LVAD implantation (100-day non-survivors) and those who survived for more than 100 days after LVAD implantation (100-day survivors) among patients with preoperative PCPS, the 100-day non-survivors required inotropic support for right ventricular dysfunction more frequently as compared with the 100-day survivors (80% vs. 20%, P=0.0403), while the total bilirubin level at 1 month after LVAD implantation was significantly higher in the 100-day non-survivors (11.4±9.7 mg/dl vs. 1.4±1.2 mg/dl, P=0.0031). In contrast, the average duration of PCPS before LVAD implantation was similar between 100-day survivors and non-survivors (5.6±6.2 days vs. 7.0±13.9 days, P=0.6498). We speculate that more aggressive mechanical right ventricular support for patients with worse postoperative right ventricular function may improve the prognosis of high-risk patients with preoperative PCPS.

In order to avoid postoperative right ventricular failure, we have considered a broad spectrum of preventative measures and maneuvers. Intraoperatively, we attempt to avoid cardioplegic arrest as much as possible to reduce ischemic insult to the right ventricle, and it was applied in only 9 of the present patients who required concomitant procedures. In addition, if tricuspid regurgitation is greater than mild and postoperative right ventricular failure is anticipated, we perform a tricuspid annuloplasty to increase forward flow from the right ventricle. We also place venting cannulae in the pulmonary artery to prevent congestion of pulmonary circulation, when anastomosing an apical cuff on a beating heart. When weaning from CPB, we utilize inotropes, PDEi, and nitric oxide inhalation to maintain adequate LVAD flow. Preoperative cardiac index $<2.2\,L\cdot min^{-1}\cdot m^{-2}$ is reported to be the most significant predictor of mechanical right ventricular support in LVAD implantation,[17] and that index was below that level in 49% of the present patients without preoperative PCPS. The intraoperative and postoperative management protocol, however, allowed all of the patients without preoperative PCPS to maintain an adequate cardiac output without mechanical right ventricular support at 1 month after LVAD implantation (**Table 5**).

Study Limitations

The main limitations of the present study were the retrospective nature of the analysis and the relatively small number of studied patients, especially those with an implantable device. Such a small number did not allow differentiation between the relative impacts of the different devices. Although excellent reductions in complication rates have been reported in patients who received a small rotary pump,[18] only 5 patients received such new devices in the present series, because their use is still considered as experimental in Japan. These new technologies may improve the outcome of patients with preoperative PCPS, because such new devices have fewer complications and their smaller blood-contacting surface reduces activation of inflammatory response.[19] Another limitation of the present study was patient selection. We accepted patients with PCPS when their end-organ dysfunction was improving and they were considered to be possible candidates for heart transplantation. Except for total bilirubin level, end-organ functions were similar in patients with and without preoperative PCPS in the present series (**Table 4**). This patient selection protocol may have contributed to the zero number of mortalities within 30 days and the relatively low rate of mechanical right ventricular support after LVAD implantation in the present series. It should be noted, however, that preoperative PCPS had a significant impact on long-term survival after LVAD implantation even in selected patients considered to be possible candidates for heart transplantation.

Conclusion

We found that patients with preoperative PCPS had significantly worse survival despite adequate hemodynamic support after LVAD implantation. The present results indicate that LVAD should be used for patients with end-stage heart failure, before PCPS is required for hemodynamic support.

References

1. Rao V, Oz MC, Flannery MA, Catanese KA, Argenziano M, Naka Y. Revised screening scale to predict survival after insertion of a left ventricular assist device. *J Thorac Cardiovasc Surg* 2003; **125:** 855–862.
2. Holman WL, Kormos RL, Naftel DC, Miller MA, Pagani FD, Blume E, et al. Predictors of death and transplant in patients with a mechanical circulatory support device: A multi-institutional study. *J Heart Lung Transplant* 2009; **28:** 44–50.
3. Shiga T, Kinugawa K, Hatano M, Yao A, Nishimura T, Endo M, et al. Age and preoperative total bilirubin level can stratify prognosis after extracorporeal pulsatile left ventricular assist device implantation. *Circ J* 2011; **75:** 121–128.
4. Pagani FD, Aaronson KD, Dyke DB, Wright S, Swaniker F, Bartlett RH. Assessment of an extracorporeal life support to LVAD bridge to heart transplant. *Ann Thorac Surg* 2000; **70:** 1977–1984.
5. Pagani FD, Lynch W, Swaniker F, Dyke DB, Bartlett R, Koelling T,

et al. Extracorporeal life support to left ventricular assist device bridge to heart transplant: A strategy to optimize survival and resource utilization. *Circulation* 1999; **100**(19 Suppl): II206–II210.
6. Nakatani T. Heart transplantation. *Circ J* 2009; **73**(Suppl A): A-55–A-60.
7. Lietz K, Long JW, Kfoury AG, Slaughter MS, Silver MA, Milano CA, et al. Outcomes of left ventricular assist device implantation as destination therapy in the post-REMATCH era: Implications for patient selection. *Circulation* 2007; **116:** 497–505.
8. Saito S, Matsumiya G, Sakaguchi T, Miyagawa S, Yoshikawa Y, Yamauchi T, et al. Risk factor analysis of long-term support with left ventricular assist system. *Circ J* 2010; **74:** 715–722.
9. Masai T, Sawa Y, Ohtake S, Nishida T, Nishimura M, Fukushima N, et al. Hepatic dysfunction after left ventricular mechanical assist in patients with end-stage heart failure: Role of inflammatory response and hepatic microcirculation. *Ann Thorac Surg* 2002; **73:** 549–555.
10. Johnson D, Mayers I. Multiple organ dysfunction syndrome: A narrative review. *Can J Anaesth* 2001; **48:** 502–509.
11. Plötz FB, van Oeveren W, Bartlett RH, Wildevuur CR. Blood activation during neonatal extracorporeal life support. *J Thorac Cardiovasc Surg* 1993; **105:** 823–832.
12. Magovern GJ Jr, Simpson KA. Extracorporeal membrane oxygenation for adult cardiac support: The Allegheny experience. *Ann Thorac Surg* 1999; **68:** 655–661.
13. McCarthy PM, Smedira NO, Vargo RL, Goormastic M, Hobbs RE, Starling RC, et al. One hundred patients with the HeartMate left ventricular assist device: Evolving concepts and technology. *J Thorac Cardiovasc Surg* 1998; **115:** 904–912.
14. Ochiai Y, McCarthy PM, Smedira NG, Banbury MK, Navia JL, Feng J, et al. Predictors of severe right ventricular failure after implantable left ventricular assist device insertion: Analysis of 245 patients. *Circulation* 2002; **106**(Suppl 1): I198–I202.
15. Kavarana MN, Pessin-Minsley MS, Urtecho J, Catanese KA, Flannery M, Oz MC, et al. Right ventricular dysfunction and organ failure in left ventricular assist device recipients: A continuing problem. *Ann Thorac Surg* 2002; **73:** 745–750.
16. Kirsch M, Vermes E, Radu C, Streich B, Nakashima K, Mekontso-Dessap A, et al. Impact of preoperative hemodynamic support on early outcome in patients assisted with paracorporeal Thoratec ventricular assist device. *Eur J Cardiothorac Surg* 2008; **34:** 262–267.
17. Fitzpatrick JR 3rd, Frederick JR, Hsu VM, Kozin ED, O'Hara ML, Howell E, et al. Risk score derived from pre-operative data analysis predicts the need for biventricular mechanical circulatory support. *J Heart Lung Transplant* 2008; **27:** 1286–1292.
18. Miller LW, Pagani FD, Russell SD, John R, Boyle AJ, Aaronson KD, et al. Use of a continuous-flow device in patients awaiting heart transplantation. *N Engl J Med* 2007; **357:** 885–896.
19. George I, Colley P, Russo MJ, Martens TP, Burke E, Oz MC, et al. Association of device surface and biomaterials with immunologic sensitization after mechanical support. *J Thorac Cardiovasc Surg* 2008; **135:** 1372–1379.

Tmem100, an ALK1 receptor signaling-dependent gene essential for arterial endothelium differentiation and vascular morphogenesis

Satoshi Somekawa[a,b], Keiichi Imagawa[a], Hisaki Hayashi[c], Masahide Sakabe[c], Tomoko Ioka[c], Genki E. Sato[c], Ken Inada[c], Takaaki Iwamoto[d], Toshio Mori[d], Shiro Uemura[a], Osamu Nakagawa[c,1], and Yoshihiko Saito[a,b]

[a]First Department of Internal Medicine, [b]Department of Regulatory Medicine for Blood Pressure, Nara Medical University, Kashihara, Nara, 634-8522, Japan; and [c]Laboratory for Cardiovascular System Research and [d]Radioisotope Research Center, Nara Medical University Advanced Medical Research Center, Kashihara, Nara, 634-8521, Japan

Edited by Eric N. Olson, University of Texas Southwestern Medical Center, Dallas, TX, and approved June 12, 2012 (received for review May 1, 2012)

Members of the transforming growth factor-β superfamily play essential roles in various aspects of embryonic development and physiological organ function. Among them, bone morphogenetic protein (BMP) 9 and BMP10 regulate embryonic vascular development by activating their endothelial receptor ALK1 (activin receptor-like kinase 1, also called Acvrl1). ALK1-mediated intracellular signaling is implicated in the etiologies of human diseases, but their downstream functional proteins are largely unknown. In this study, we identified *Tmem100*, a gene encoding a previously uncharacterized intracellular transmembrane protein, to be an embryonic endothelium-enriched gene activated by BMP9 and BMP10 through the ALK1 receptor. *Tmem100* null mice showed embryonic lethality due to impaired differentiation of arterial endothelium and defects of vascular morphogenesis, which phenocopied most of the vascular abnormalities observed with the *Acvrl1/Alk1* deficiency. The activity of Notch- and Akt-mediated signaling, which is essential for vascular development, was down-regulated in *Tmem100* null mice. *Cre*-mediated deletion of *Tmem100* in endothelial cells was sufficient to recapitulate the null phenotypes. These data indicated that TMEM100 may play indispensable roles downstream of BMP9/BMP10-ALK1 signaling during endothelial differentiation and vascular morphogenesis.

Formation of the cardiovascular network is essential for proper embryonic development, and neovascularization is associated with various adult diseases, such as ischemic heart diseases, retinopathy, and cancer, acting either protectively or deteriorately in those pathological states (1, 2). At early embryonic stages, vasculogenesis occurs as a de novo organization of endothelial cell plexus. A series of processes for vascular remodeling and maturation follows, including an initial phase of endothelial cell migration, proliferation, and tubular reorganization, collectively called angiogenesis, and a maturation phase when the structure of blood vessels is established by the stabilization of endothelial cells, acquirement of arterial or venous identity, and recruitment of mural cells to vascular walls (1, 2).

A variety of cellular signaling pathways controlling vascular development involve cytokines and growth factors, such as vascular endothelial growth factors (VEGFs), angiopoietins, transforming growth factor β (TGF-β), and bone morphogenetic proteins (BMPs) (3, 4). Among them, BMP9 and BMP10 act mainly through an endothelium-specific ALK1 (activin receptor-like kinase 1) receptor and promote arterial endothelial maturation and quiescence (5–7). Targeting disruption of the genes for the ALK1 receptor, a type III coreceptor endoglin, and downstream signaling components such as Tak1/Map3k7 caused embryonic lethality with remarkably similar defects of arterial endothelium differentiation and vascular morphogenesis (8–11). Despite clear demonstration of its critical roles in embryonic development, endothelial functional proteins downstream of the BMP9/BMP10-ALK1 signaling pathway remained unclear.

In a microarray screen to search for endothelial genes downstream of BMP9/BMP10-ALK1 signaling, we found that the expression of *Tmem100*, a gene encoding an intracellular transmembrane protein of unknown functions, was markedly augmented by BMP9 and BMP10. It was recently reported that *Tmem100* mRNA expression significantly decreased in the lung of *Acvrl1/Alk1* conditional knockout mice and that *Tmem100* drove endothelial-enriched expression of lacZ reporter in mouse embryos (12). In this paper, we demonstrated that *Tmem100* null mice and endothelial-specific *Tmem100* knockout mice showed fatal defects of arterial endothelium differentiation and vascular morphogenesis, which are virtually identical to the abnormalities due to the *Acvrl1/Alk1* deficiency. These results suggest that TMEM100 may play essential roles as a downstream target protein of BMP9/BMP10-ALK1 signaling in embryonic vascular development.

Results

***Tmem100*: An Arterial Endothelium-Enriched Gene Downstream of BMP9/BMP10-ALK1 Signaling.** In an attempt to identify endothelial genes downstream of BMP9/BMP10-ALK1 signaling, we first analyzed whether human umbilical artery endothelial cells (HUAEC) responded to the treatment with various TGF-β–related factors. Among several ligands tested, BMP9 potently stimulated the phosphorylation of Smad1/5/8 (Fig. S1 *A* and *B*). We then compared gene expression profiles of BMP9-treated HUAEC and control cells by an RNA microarray analysis (Fig. S1*C*). In addition to known BMP9-target genes such as *SMAD6, SMAD7*, *ID1*, and *ID2*, we found that *TMEM100* showed a marked activation of mRNA expression by the BMP9 treatment (Fig. 1*A*). Quantitative RT-PCR and Western blot analysis confirmed a dose-dependent induction of the *TMEM100* expression by BMP9, up to more than 100-fold (Fig. 1*A*). Similar levels of activation were observed with BMP10 (Fig. S1*D*), and those effects were significantly inhibited by knockdown of *ACVRL1/ALK1*, *BMPR2*, and *SMAD4* (Fig. 1*B* and Fig. S1*E*). These results indicated that BMP9/BMP10-induced *TMEM100* expression occurred through the ALK1/BMPR2 receptor complex and Smad-mediated transcriptional regulation.

TMEM100 is a gene encoding a protein with two putative transmembrane domains, but its physiological significance has not been described. The structure of TMEM100 protein is highly

Author contributions: S.S., O.N., and Y.S. designed research; S.S., K. Imagawa, H.H., M.S., T. Ioka, G.E.S., K. Inada, T. Iwamoto, and T.M. performed research; S.S., S.U., O.N., and Y.S. analyzed data; and S.S., O.N., and Y.S. wrote the paper.

The authors declare no conflict of interest.

This article is a PNAS Direct Submission.

[1]To whom correspondence should be addressed. E-mail: nakagawa-nmu@umin.org

This article contains supporting information online at www.pnas.org/lookup/suppl/doi:10.1073/pnas.1207210109/-/DCSupplemental.

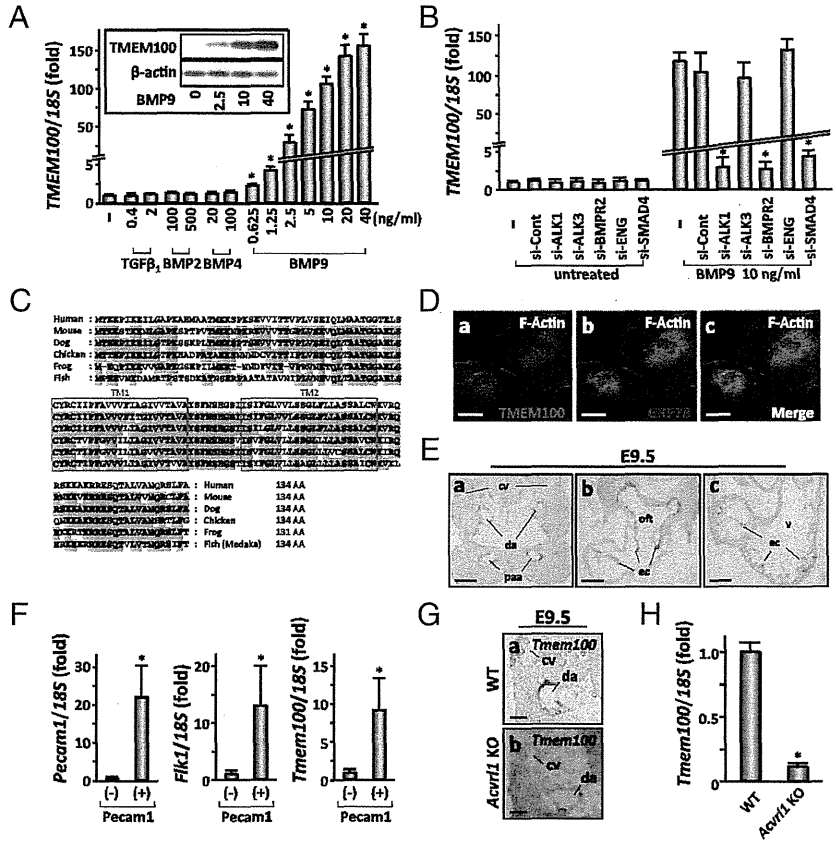

Fig. 1. *Tmem100*: an arterial endothelium-enriched gene downstream of BMP9/BMP10-ALK1 signaling. (*A*) BMP9 markedly increases *TMEM100* mRNA expression at 24 h in a dose-dependent manner. Quantitative RT-PCR analysis is shown. Fold increase relative to the untreated cells is shown with SD. (*Inset*) Western blot result shows a dose-dependent increase in TMEM100 protein expression. –, untreated. (*B*) BMP9-induced *TMEM100* mRNA expression is inhibited by pretreatment with ACVRL1/ALK1 siRNA (si-ALK1), BMPR2 siRNA (si-BMPR2), or SMAD4 siRNA (si-SMAD4), but not with BMPR1A/ALK3 siRNA (si-ALK3), Endoglin siRNA (si-ENG), or control siRNA (si-Cont). Quantitative RT-PCR is shown. –, untreated. (*C*) Amino acid sequences of TMEM100 from various species. Boxes represent two putative transmembrane (TM) domains. Residues conserved with the human sequence are shaded in gray. (*D*) TMEM100 protein predominantly resides in the perinuclear region overlapping endoplasmic reticulum marked by anti-GRP78/HSPA5 antibody. Immunocytochemistry of HUAEC transfected with a TMEM100-FLAG expression plasmid is shown. (*E*) *Tmem100* mRNA is expressed specifically in arterial endothelial cells of pharyngeal arch artery (paa) and dorsal aorta (da) as well as in endocardium (ec), but not in cardinal vein (cv), at E9.5. In situ hybridization is shown. oft, outflow tract; v, ventricle. (*F*) *Tmem100* expression is enriched in endothelial cells also at earlier developmental stages. Shown is FACS sorting of Pecam1-positive cells from E8.5 embryos followed by quantitative RT-PCR. *Pecam1* and *Kdr/Flk1* expression was examined to confirm proper selection of the endothelial population. (*G*) *Tmem100* expression in dorsal aorta is reduced in *Acvrl1/Alk1* null embryos at E9.5. In situ hybridization is shown. (*H*) *Tmem100* expression significantly decreases in the yolk sac of *Acvrl1/Alk1* null mice at E9.5. Quantitative RT-PCR is shown. In *A*, *B*, *F*, and *H*, asterisks indicate data with statistical significance (*$P < 0.05$). (Scale bars: *D*, 10 μm; *E*, 50 μm; and *G*, 20 μm.)

conserved from fish to humans, especially in its putative transmembrane domains (Fig. 1*C*); however, no structurally related family of proteins was found in any species, indicating that TMEM100 represents a previously uncharacterized entity of functional proteins. Levels of endogenous TMEM100 expression in HUAEC were below detection limits in immunocytochemical analyses, whereas TMEM100 protein expressed using a mammalian expression plasmid resided in the perinuclear region marked by endoplasmic reticulum (ER) proteins such as GRP78/HSPA5 (Fig. 1*D* and Fig. S2*A*). Endogenous TMEM100 protein in BMP9-treated HUAEC was recovered to the subcellular membrane fraction and was enriched in the ER microsome (Fig. S2 *B* and *C*). In adult mice, *Tmem100* was most abundantly expressed in the lung with a lower level of expression in the brain, heart, and muscle (Fig. S2*D*). In mouse embryos, *Tmem100* mRNA was detected from embryonic day (E) 8.5 (Fig. S2*E*) and was enriched in arterial endothelium and endocardium (Fig. 1*E* and see Fig. S4*A*). Quantitative RT-PCR confirmed the enrichment of *Tmem100* mRNA in the platelet/endothelial cell adhesion molecule 1 (Pecam1)-positive endothelial cell population sorted from E8.5 embryos (Fig. 1*F*). Consistent with ALK1-mediated *Tmem100* expression in HUAEC (Fig. 1 *A* and *B*) and the previous report (12), *Tmem100* mRNA expression in arterial endothelium was significantly reduced in *Acvrl1/Alk1* null embryos (Fig. 1 *G* and *H*).

These results prompted us to examine functional significance of TMEM100 in vascular differentiation and morphogenesis during development.

Embryonic Lethality by Targeted Disruption of *Tmem100*. We generated *Tmem100*-deficient mice in which exon 3 encoding the entire coding region was replaced with a lacZ-neo cassette (Fig. S3 *A–C*). Mice heterozygous for the *Tmem100* mutation survived to adulthood and were fertile. LacZ reporter driven by the *Tmem100* locus (*Tmem100-lacZ*) was predominantly expressed in developing arteries, including dorsal aorta and pharyngeal arch; intersomitic, umbilical, and vitelline arteries; and endocardium (Fig. 2 *A* and *B* and Fig. S4 *B–D*). Vascular expression of *Tmem100-lacZ* overlapped with that of lacZ reporter knocked into the *Acvrl1/Alk1* locus (Fig. 2 *A* and *B*) and was observed in

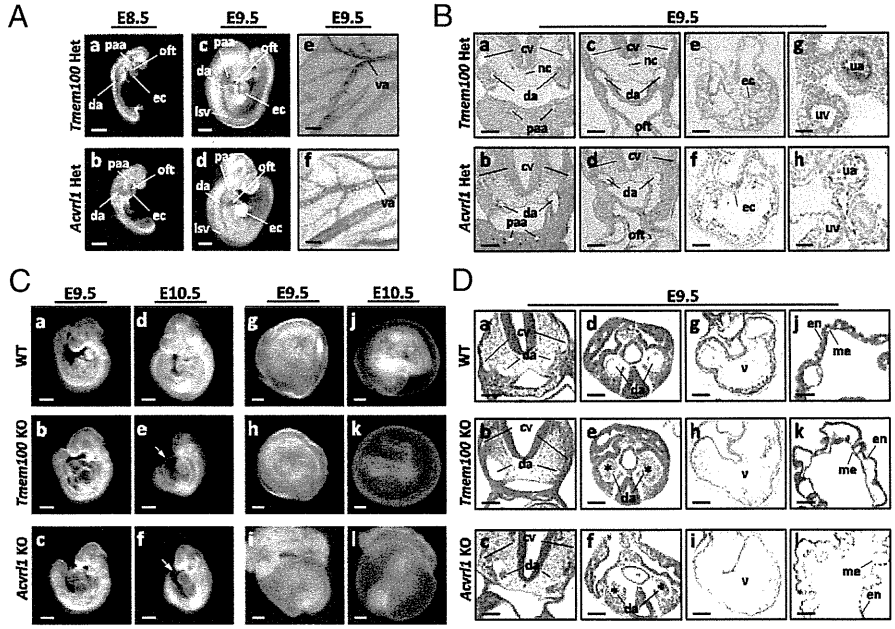

Fig. 2. *Tmem100* and *Acvrl1/Alk1*: arterial expression of knock-in lacZ reporter and angiogenesis defects in null embryos. (*A* and *B*) Knock-in lacZ reporter activity is detected in major arteries and endocardium in both *Tmem100* and *Acvrl1/Alk1* heterozygous mice. Sections counterstained with nuclear fast red are shown in *B*. (*C*) *Tmem100* null embryos die in utero, showing cardiac dysmorphogenesis and enlargement at E9.5, massive pericardial effusion (arrow) and severe growth retardation at E10.5, and absence of large vitelline vessels in the yolk sac at E10.5. These phenotypes are also observed in *Acvrl1/Alk1* null embryos. (*D*) *Tmem100* null and *Acvrl1/Alk1* null embryos have remarkably similar defects of cardiovascular morphogenesis. Paired dorsal aortas show marked dilatation and narrowing, and clumps of blood cells are frequently seen in the caudal region (asterisk). Mural layers surrounding the aorta and myocardial wall are thinner and ventricular trabeculation is not formed well. The yolk sac shows detachment of endodermal (en) and mesodermal (me) layers and abnormal vessel dilatation. H&E staining at E9.5 is shown. cv, cardinal vein; da, dorsal aorta; isv, intersomitic vessel; nc, notochord; oft, outflow tract; paa, pharyngeal arch artery; ua, umbilical artery; uv, umbilical vein; v, ventricle; va, vitelline artery. (Scale bars: *A*, *a–d*, and *C*, 200 μm; *A*, *e* and *f*, *B*, a–f, and *D*, *a–i*, 50 μm; and *B*, *g* and *h*, and *D*, *j–l*, 20 μm.)

the endothelial layer of dorsal aorta but not in smooth muscle cells (Fig. S4 *C* and *D*). At later embryonic stages, *Tmem100-lacZ* expression was also detected in the limb buds, somites, and other tissues (Fig. S4*B*). In the adult lung, *lacZ* reporter was expressed in vascular endothelial cells as well as in alveolar cells (Fig. S4*E*).

Breeding of heterozygous mice revealed a significant deviation from expected inheritance, and no surviving embryos were recovered at and after E11.0 (Fig. S3*D*). *Tmem100* null embryos at E10.5 were strongly affected, showing abnormal cardiac morphology, massive pericardial effusion, and growth retardation (Fig. 2*C*), suggesting that cardiovascular failure caused embryonic lethality of *Tmem100* null mice.

Vascular Defects in *Tmem100* Null Mice. *Tmem100* null embryos showed no detectable phenotypes until E8.5, and the formation of primitive vasculature appeared normal (Fig. S5*A*). Earliest signs of deficiency were observed in the vasculature at E9.0–9.5. The yolk sac of *Tmem100* null embryos showed reduction of vitelline circulation (Fig. 2*C*). Consistently, *Tmem100* null embryos displayed a variety of severe abnormalities in vascular morphology, as shown in Fig. 2*D*. One of the paired dorsal aortae frequently showed a marked dilatation with a narrowing or closure on the opposite side, and clumps of blood cells were often observed in the caudal region, which is likely to be due to vascular obstruction. Cardiac myocardium was thinner, and the yolk sacs showed detachment of endodermal and mesodermal layers and abnormal vessel dilatation (Fig. 2*D*).

Whole-mount Pecam1 staining revealed abnormally coarse vascular patterns, indicative of impaired vascular remodeling (Fig. 3*A*), and India ink injection identified arteriovenous malformation from dorsal aorta toward sinus venosus in *Tmem100* null embryos (Fig. 3*B* and Fig. S5*B*). These phenotypes of *Tmem100* null embryos were mostly identical to those observed in *Acvrl1/Alk1* null embryos (Fig. 2 *C* and *D* and Fig. S6*A*) and reported in previous studies (8, 9).

Defects of Arterial Differentiation in *Tmem100* Null Embryos. ALK1-mediated signaling is implicated in establishing arterial identity of vascular endothelial cells (8, 9). Indeed, the expression of arterial marker genes *Efnb2* and *Gja5/Cx40* was significantly decreased in dorsal aorta of *Tmem100* null embryos as early as E8.5 (Fig. 3 *C* and *D*). In contrast, expression of *Cdh5* (encoding VE-cadherin), *Kdr/Flk1*, and *Pecam1* was maintained (Fig. 3 *C–E*), suggesting that arterial specification is compromised by *Tmem100* deficiency. Upon normal arterial maturation, mural smooth muscle precursors marked by Sm22 are recruited (1, 2); however, the *Sm22/Tagln* expression around the dorsal aorta was significantly reduced in *Tmem100* null embryos (Fig. 3*F*). These defects of arterial differentiation and maturation were also observed in *Acvrl1/Alk1* null mice (Fig. S6 *B–E*).

Down-Regulation of Endothelial Signaling Pathways in *Tmem100* Null Embryos. To begin to understand mechanisms of vascular abnormalities caused by the *Tmem100* deficiency, we performed a microarray analysis using the yolk sac, which is a vascular-rich tissue with obvious null phenotypes (Fig. S7*A*). We observed a significant decrease in the expression of arterial markers, such as *Efnb2*, *Gja4/Cx37*, and *Gja5/Cx40*, and an increase in vein-specific *Ephb4* expression in the *Tmem100* null yolk sac (Fig. 4*A* and Fig. S7*B*), which is consistent with our notion that *Tmem100* is essential for arterial endothelium differentiation.

We also found that the expression of Notch downstream genes *Hrt1/Hey1*, *Hrt2/Hey2*, *Hrt3/Heyl*, and *Hes5* (13, 14) was signifi-

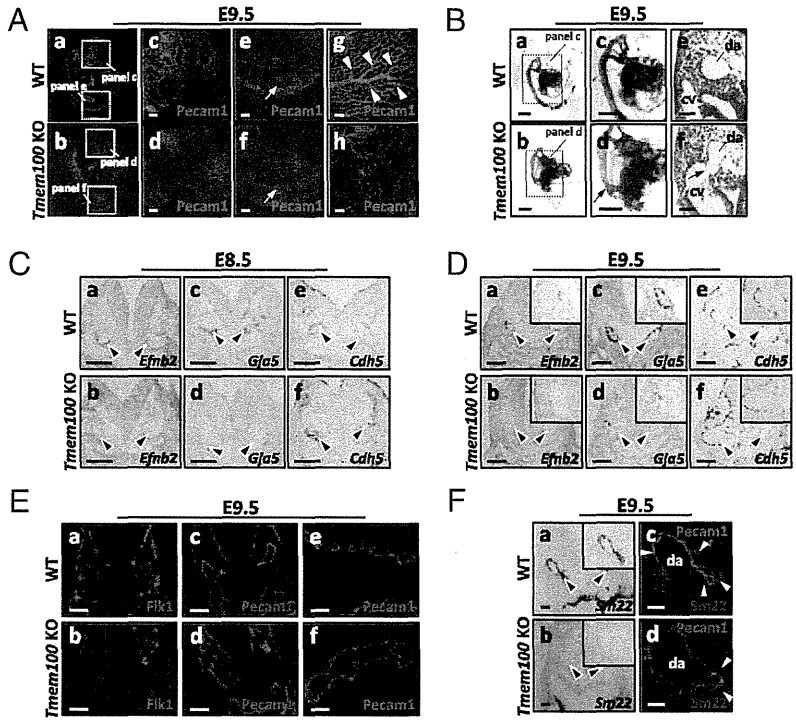

Fig. 3. Impairment of vascular remodeling and arterial endothelium differentiation in *Tmem100* null embryos. (*A*) Impaired vascular remodeling is visualized by whole-mount Pecam1 immunostaining in the *Tmem100* null embryos (*b*, *d*, and *f*) and yolk sac (*h*). Arrows indicate intersomitic vessels. Arrowheads indicate highly organized vascular branches in the wild-type yolk sac. *a–f* are shown with nuclear DAPI stain. (*B*) Abnormal vascular connections (arrow) between dorsal aorta and cardinal veins are observed in null embryos. Shown is microangiography by India ink injection and H&E staining. (*C* and *D*) Expression of arterial endothelium marker genes *Efnb2* and *Gja5/Cx40* diminishes in dorsal aorta (arrowheads) of *Tmem100* null embryos at E8.5 (*C*) and E9.5 (*D*), whereas maintenance of *Cdh5* expression indicates existence of endothelial layers. In situ hybridization is shown. (*E*) Flk1 and Pecam1 expression is preserved in dorsal aorta of *Tmem100* null embryo (*b* and *d*) and yolk sac vasculature (*f*). Immunohistochemistry with nuclear DAPI stain is shown. (*F*) Expression of *Sm22/Tagln* mRNA and SM22 protein in the mural layers of dorsal aorta is significantly reduced in *Tmem100* null embryos (arrowheads). In situ hybridization (*a* and *b*) and immunohistochemistry with nuclear DAPI stain (*c* and *d*) are shown. *Insets* in *D* and *F* show magnified views of dorsal aorta. (Scale bars: *A*, *C*, *D*, and *E*, *a–d*, 50 μm; *B*, *a–d*, 200 μm; and *B*, *e* and *f*, *E*, *e* and *f*, and *F*, 20 μm.)

cantly decreased in *Tmem100* null yolk sac (Fig. 4*A* and Fig. S7*C*). Because Notch signaling was known to be essential for arterial differentiation (1, 2, 15), we further examined whether the activity of Notch signaling is down-regulated in *Tmem100* null embryos. Upon activation by the ligands such as Delta and Jagged, the intracellular domain of Notch receptors, NICD, is enzymatically cleaved and translocated to the nucleus, where it forms a transcriptional activator complex with RBP-J and other cofactors (14). Western blot analysis demonstrated a significant decrement of NICD expression in *Tmem100* null embryos and yolk sac (Fig. 4*B*). Immunohistochemical staining using an anti–NICD-specific antibody indicated that down-regulation of NICD expression was specific to the arterial endothelium and endocardium and was not observed in other Notch-regulated tissues such as somite and neural tube (Fig. 4*C*). The total amount of Notch receptors, which was examined using an antibody recognizing both full-length Notch receptors and NICD, appeared unchanged (Fig. 4*D*). Furthermore, the expression of Notch-target transcription factor Hrt2/Hey2 was significantly decreased in the vasculature of *Tmem100* null embryos, whereas its expression in the cardiac muscle was unaltered (Fig. 4*E*).

In addition, we observed a decrease in Akt phosphorylation in *Tmem100* null embryos and yolk sac (Fig. 4*B*). Consistently, the expression of *Klf2* and *eNOS/Nos3* (Fig. 4*A*) and the cleavage of Presenilin-1 (Ps1) (Fig. 4*F*), which can be activated by Akt signaling (16–18), were suppressed in null embryos and yolk sac, suggesting down-regulation of Akt-mediated signaling important for endothelial survival, migration, and homeostasis. Importantly, dysregulation of Notch and Akt signaling was also observed in *Acvrl1/Alk1* null mice (Fig. S6 *F–K*).

In contrast, other signaling pathways implicated in embryonic vascular development did not appear compromised (1, 2, 19–22). The levels of ERK and Smad1/5/8 phosphorylation did not alter in *Tmem100* null embryos and yolk sac (Fig. S7 *D–F*). Components of Angiopoietin, Hedgehog, Semaphorin, and fibroblast growth factor signaling pathways and their downstream target genes did not show aberrant expression in *Tmem100* null yolk sac (Fig. S7*C*). These data suggested that the *Tmem100* deficiency caused impairment of arterial differentiation and morphogenesis through, at least in part, down-regulation of Notch- and Akt-mediated signaling.

Embryonic Vascular Defects by Cre-Mediated Deletion of *Tmem100* in Endothelial Cells. We further examined phenotypes of the mice with *Tek-Cre*–mediated endothelial cell-specific deletion of the *Tmem100* gene (Fig. S8 *A–D*). Endothelial-specific deletion of *Tmem100* caused vascular defects remarkably similar to those observed in global *Tmem100* null mice and embryonic lethality around E11.0 (Fig. S8 *E* and *F*). Expression of arterial endothelium-specific genes and a vascular smooth muscle marker SM22 apparently decreased, and Notch- and Akt-mediated signaling was down-regulated also by the endothelial-specific *Tmem100* deletion (Fig. S9 *A–D*). These results indicated that the endothelial expression of *Tmem100* is essential for arterial differentiation and embryonic development.

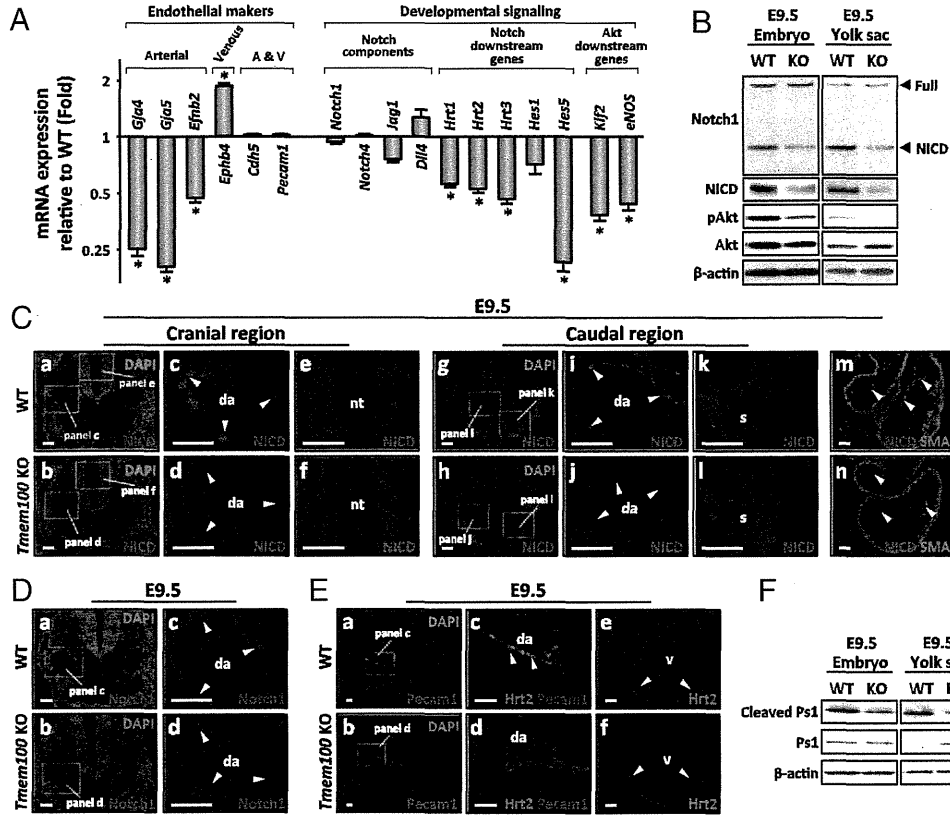

Fig. 4. Notch- and Akt-mediated signaling pathways are down-regulated in *Tmem100* null embryos and yolk sac. (*A*) Expression of arterial endothelium markers, Notch downstream genes, and Akt downstream genes markedly decreases in *Tmem100* null yolk sac at E9.5. Expression of a venous endothelium marker, *Ephb4*, is significantly up-regulated. Quantitative RT-PCR is shown. (*B*) The amount of the intracellular domain of Notch receptor (NICD) and phosphorylated Akt significantly decreases in *Tmem100* null embryos and yolk sac at E9.5, whereas that of full-length Notch1 receptor and total Akt remains unchanged. Western blot analysis is shown. (*C*) NICD expression markedly decreases in dorsal aorta (da) and endocardium (arrowheads in *d*, *j*, and *n*), but not in the neural tube (nt) and somites (s) (*f* and *l*), of E9.5 null embryos. Immunohistochemistry using a NICD-specific antibody is shown. *a*, *b*, *g*, *h*, *m*, and *n* are shown with nuclear DAPI stain. (*D*) Total amount of Notch receptors does not decrease in vascular endothelium of null embryos. Immunohistochemistry using an antibody recognizing full-length Notch receptors and NICD is shown. *a* and *b* are shown with nuclear DAPI stain. (*E*) Expression of Hrt2, a Notch downstream transcription factor, significantly decreases in the vasculature of *Tmem100* null embryos (*d*), whereas its expression in cardiac muscle was unchanged (*f*). Immunohistochemistry is shown. *a* and *b* are shown with nuclear DAPI stain. (*F*) Cleaved Presenilin-1 (Ps1) decreases in null embryos and yolk sac at E9.5. Western blot analysis is shown. (Scale bars in *C–E*, 20 μm.)

Discussion

In searching for genes involved in the regulation of endothelial differentiation and vascular development, we identified *Tmem100* to be a gene activated downstream of BMP9/BMP10-ALK1 signaling. *Tmem100* and *Acvrl1/Alk1* were expressed in arterial endothelial cells during vascular development in mouse embryos, and their targeting disruption caused embryonic lethality with remarkably similar abnormalities of arterial endothelium differentiation and vascular morphogenesis. *Tmem100* expression significantly decreased in *Acvrl1/Alk1* null embryos, which is consistent with down-regulation of *Tmem100* expression in the adult lung of *Acvrl1/Alk1* conditional knockout mice (12). It has not been studied whether BMP9 and BMP10 are major regulators of *Tmem100* expression in vivo. *Bmp10* null mice show impaired cardiac growth but not defects of angiogenesis (23), whereas the phenotypes of *Gdf2* (encoding BMP9) knockout mice have not been reported. Examining whether the mice null for both *Gdf2* and *Bmp10* show embryonic vascular defects will provide further insights into in vivo regulatory mechanisms of *Tmem100* expression.

Notch-mediated signaling was suppressed in arterial endothelium of *Tmem100* null embryos as well as in endothelial-specific *Tmem100* knockout embryos. We also found that Notch signaling was down-regulated in *Acvrl1/Alk1* null embryos. Notch receptors and ligands are enriched in arterial but not venous endothelium of mouse embryos, and target disruption of Notch signaling components such as *Notch1*, *Notch4*, *Dll4*, *Rbpj*, *Hrt1/Hey1*, and *Hrt2/Hey2* revealed that Notch activity is crucial for promoting arterial cell fate (1, 2, 15). Impairment of endothelial Notch signaling affects vascular smooth muscle cell recruitment or differentiation during arterial maturation (24–26), which was observed in *Tmem100* and *Acvrl1/Alk1* knockout mice in the present study. In addition to Notch signaling, the activities of Akt kinase and Ps1 protease appeared repressed in *Tmem100* and *Acvrl1/Alk1* knockout embryos. It was reported that Akt enhances Ps1-mediated Notch cleavage (16, 27) and that Ps1 provokes Akt activation in turn (28). The signaling relay or mutual interaction involving Akt, Ps1, and Notch might play a role in the pathogenesis of vascular defects by the *Tmem100* and *Acvrl1/Alk1* deficiency.

A number of biological stimuli including fluid shear stress could influence Akt- and Notch-mediated signaling as a result of insufficient circulation (1, 2, 15). Markers of arterial endothelium differentiation, however, became down-regulated before apparent structural abnormalities in *Tmem100* null embryos, suggesting a possibility that TMEM100 is directly involved in acquiring arterial cell fate. Previous studies reported *Tmem100*

expression in embryonic vasculature and the adult lung, prostate, and kidney in humans and mice (12, 29, 30), but cellular functions of TMEM100 have not been investigated. We found that TMEM100 protein was mainly localized in ER, but not in plasma membrane, of cultured endothelial cells. It is tempting to speculate that TMEM100 works for posttranslational protein modification or intracellular sorting in the membrane of ER and surrounding structures. Elucidating molecular functions of TMEM100 is essential to clarify how TMEM100 conveys the BMP9/BMP10-ALK1 signals toward the downstream signaling cascade for proper endothelial differentiation.

Mutations in *ACVRL1/ALK1*, *BMPR2*, *ENG*, or *SMAD4* cause hereditary hemorrhagic telangiectasia as well as pulmonary arterial hypertension in humans (31, 32). *TMEM100* might be involved in the mechanisms of these diseases as an additional causative gene or a modifier. At late embryonic and adult stages, *Tmem100* expression appears to be not restricted to vascular endothelial cells. Studying the significance of TMEM100 may lead to a better understanding of human diseases in the cardiovascular system and other organs.

Materials and Methods

Cell Culture and Microarray Analysis. HUAEC (Takara Bio) were precultured in Endothelial Basal Medium 2 medium with 0.2% FBS for 3 h and treated with TGF-β superfamily ligands (R&D Systems) for 24 h. siRNA was electroporated to HUAEC 36 h before the BMP9 or BMP10 treatment. Other cell culture experiments were performed using standard procedures.

Two-color microarray analyses using the human and mouse whole-genome 4x44K v2 oligo microarray systems (Agilent Technologies) were performed to examine mRNA expression profiles of BMP9-treated HUAEC and the yolk sac of *Tmem100* null mice, respectively.

Generation of *Tmem100* Null Mice. The *Tmem100*-lacZ targeting vector was constructed using a BAC clone containing the *Tmem100* locus genomic DNA (BACPAC Resources) and was electroporated into C57BL/6 embryonic stem cells for homologous recombination (Fig. S3*A*). A correctly targeted clone, as identified by Southern blot analysis, was injected into BALB/c blastocysts. Chimeras were bred to obtain heterozygous mice that carry the targeted *Tmem100* locus in their germ line. The floxed PGK-neo cassette was removed by breeding with a *CAG-Cre* transgenic line. All breeding was done with mice under the C57BL/6 genetic background. Procedures to generate mice for conditional *Tmem100* deletion are described in *SI Materials and Methods*. All animal experiments were approved by the institutional committee.

Biochemical, Histological, and Anatomical Analyses. Quantitative RT-PCR, Northern blot analysis, Western blot analysis, in situ hybridization, immunohistochemistry, and lacZ staining were performed using standard procedures. A rabbit polyclonal antibody generated against a carboxyl-terminal 27-aa fragment of mouse TMEM100 protein was used for Western blot analysis of HUAEC. Details of PCR primers, Northern probe, and primary antibodies are described in *SI Materials and Methods*. Microangiography was performed by India ink injection to the outflow tract of mouse embryos.

ACKNOWLEDGMENTS. The authors thank Drs. E. Olson, J. Hill, and P. ten Dijke for profitable advice and support. The authors also thank Drs. A. Wanaka, K. Tatsumi, H. Yamagishi, K. Uchida, H. Bannai, H. Kurihara, R. Asai, S. Itoh, F. Itoh, T. Morioka, and M. Itoh for experimental information and Ms. M. Ikugawa, T. Fujita, Y. Yoshioka, and M. Sakaida for technical assistance. This study was supported in part by grants from the Ministry of Education, Culture, Sports, Science, and Technology (to O.N., S.S., H.H., M.S., and Y.S.); grants from the Astellas Foundation for Research on Metabolic Disorders, the Mitsubishi Pharma Research Foundation, the Miyata Cardiac Research Promotion Foundation, Novartis Foundation (Japan) for the Promotion of Science, Suzuken Memorial Foundation, the Takeda Science Foundation, The Mother and Child Health Foundation, The Naito Foundation, The Smoking Research Foundation, and the Uehara Memorial Foundation (to O.N.); grants from the Banyu Life Science International Foundation and Takeda Science Foundation (to S.S.); grants from the Takeda Science Foundation, The Ichiro Kanahara Foundation, and The Nakatomi Foundation (to H.H.); a grant from Japan Heart Foundation (to M.S.); and a research grant for Cardiovascular Diseases (20A-3) from the Ministry of Health, Labor and Welfare (to Y.S.).

1. Potente M, Gerhardt H, Carmeliet P (2011) Basic and therapeutic aspects of angiogenesis. *Cell* 146:873–887.
2. Eilken HM, Adams RH (2010) Dynamics of endothelial cell behavior in sprouting angiogenesis. *Curr Opin Cell Biol* 22:617–625.
3. David L, Feige JJ, Bailly S (2009) Emerging role of bone morphogenetic proteins in angiogenesis. *Cytokine Growth Factor Rev* 20:203–212.
4. Pardali E, Goumans MJ, ten Dijke P (2010) Signaling by members of the TGF-beta family in vascular morphogenesis and disease. *Trends Cell Biol* 20:556–567.
5. David L, Mallet C, Mazerbourg S, Feige JJ, Bailly S (2007) Identification of BMP9 and BMP10 as functional activators of the orphan activin receptor-like kinase 1 (ALK1) in endothelial cells. *Blood* 109:1953–1961.
6. Scharpfenecker M, et al. (2007) BMP-9 signals via ALK1 and inhibits bFGF-induced endothelial cell proliferation and VEGF-stimulated angiogenesis. *J Cell Sci* 120:964–972.
7. Suzuki Y, et al. (2010) BMP-9 induces proliferation of multiple types of endothelial cells in vitro and in vivo. *J Cell Sci* 123:1684–1692.
8. Urness LD, Sorensen LK, Li DY (2000) Arteriovenous malformations in mice lacking activin receptor-like kinase-1. *Nat Genet* 26:328–331.
9. Oh SP, et al. (2000) Activin receptor-like kinase 1 modulates transforming growth factor-beta 1 signaling in the regulation of angiogenesis. *Proc Natl Acad Sci USA* 97:2626–2631.
10. Li DY, et al. (1999) Defective angiogenesis in mice lacking endoglin. *Science* 284:1534–1537.
11. Jadrich JL, O'Connor MB, Coucouvanis E (2006) The TGF beta activated kinase TAK1 regulates vascular development in vivo. *Development* 133:1529–1541.
12. Moon EH, et al. (2010) Generation of mice with a conditional and reporter allele for Tmem100. *Genesis* 48:673–678.
13. Nakagawa O, et al. (2000) Members of the HRT family of basic helix-loop-helix proteins act as transcriptional repressors downstream of Notch signaling. *Proc Natl Acad Sci USA* 97:13655–13660.
14. Kopan R, Ilagan MX (2009) The canonical Notch signaling pathway: Unfolding the activation mechanism. *Cell* 137:216–233.
15. Swift MR, Weinstein BM (2009) Arterial-venous specification during development. *Circ Res* 104:576–588.
16. Takeshita K, et al. (2007) Critical role of endothelial Notch1 signaling in postnatal angiogenesis. *Circ Res* 100:70–78.
17. Sako K, et al. (2009) Angiopoietin-1 induces Kruppel-like factor 2 expression through a phosphoinositide 3-kinase/AKT-dependent activation of myocyte enhancer factor 2. *J Biol Chem* 284:5592–5601.
18. SenBanerjee S, et al. (2004) KLF2 is a novel transcriptional regulator of endothelial proinflammatory activation. *J Exp Med* 199:1305–1315.
19. Srinivasan R, et al. (2009) Erk1 and Erk2 regulate endothelial cell proliferation and migration during mouse embryonic angiogenesis. *PLoS ONE* 4:e8283.
20. Lechleider RJ, et al. (2001) Targeted mutagenesis of Smad1 reveals an essential role in chorioallantoic fusion. *Dev Biol* 240:157–167.
21. Yang X, et al. (1999) Angiogenesis defects and mesenchymal apoptosis in mice lacking SMAD5. *Development* 126:1571–1580.
22. Chang H, et al. (1999) Smad5 knockout mice die at mid-gestation due to multiple embryonic and extraembryonic defects. *Development* 126:1631–1642.
23. Chen H, et al. (2004) BMP10 is essential for maintaining cardiac growth during murine cardiogenesis. *Development* 131:2219–2231.
24. Morrow D, et al. (2008) Notch and vascular smooth muscle cell phenotype. *Circ Res* 103:1370–1382.
25. Fischer A, Schumacher N, Maier M, Sendtner M, Gessler M (2004) The Notch target genes Hey1 and Hey2 are required for embryonic vascular development. *Genes Dev* 18:901–911.
26. High FA, et al. (2008) Endothelial expression of the Notch ligand Jagged1 is required for vascular smooth muscle development. *Proc Natl Acad Sci USA* 105:1955–1959.
27. Yamamizu K, et al. (2010) Convergence of Notch and beta-catenin signaling induces arterial fate in vascular progenitors. *J Cell Biol* 189:325–338.
28. Baki L, et al. (2004) PS1 activates PI3K thus inhibiting GSK-3 activity and tau overphosphorylation: Effects of FAD mutations. *EMBO J* 23:2586–2596.
29. van der Heul-Nieuwenhuijsen L, Hendriksen PJ, van der Kwast TH, Jenster G (2006) Gene expression profiling of the human prostate zones. *BJU Int* 98:886–897.
30. Georgas K, et al. (2009) Analysis of early nephron patterning reveals a role for distal RV proliferation in fusion to the ureteric tip via a cap mesenchyme-derived connecting segment. *Dev Biol* 332:273–286.
31. Govani FS, Shovlin CL (2009) Hereditary haemorrhagic telangiectasia: A clinical and scientific review. *Eur J Hum Genet* 17:860–871.
32. Lowery JW, de Caestecker MP (2010) BMP signaling in vascular development and disease. *Cytokine Growth Factor Rev* 21:287–298.

Supporting Information

Somekawa et al. 10.1073/pnas.1207210109

SI Materials and Methods

Reagents. Bone marrow morphogenetic protein (BMP)2, BMP4, BMP6, BMP9, BMP10, and TGF-β1 were purchased from R&D Systems. siRNA for ACVRL1/ALK1, BMPR1A/ALK3, BMPR2, SMAD4, and negative control (si-Cont) were from Invitrogen. siRNA for Endoglin was from Applied Biosystems. Manufacturers of primary antibodies were as follows: GRP78/HSPA5, Presenilin-1, and Sm22, Abcam; Flk1 and platelet/endothelial cell adhesion molecule 1 (Pecam1), BD Biosciences; β-gal, Biogenesis; pSmad2, Calbiochem; Akt, phosphorylated (p) Akt, Calnexin, COXIV, LC3B, Notch1, Notch1-ICD, Rab5, S6, Smad1, Smad2, pSmad1/5/8, and Syntaxin6, Cell Signaling; Vimentin, Dako; cleaved Presenilin-1, Millipore; Hrt2, ProteinTech Group; HSC70 and Histone1, Santa Cruz; β-actin and smooth muscle actin, Sigma-Aldrich; and Calreticulin, Thermo.

RNA Interference. siRNA was transfected into human umbilical artery endothelial cells (HUAEC) by electroporation, using the Nucleofector kit (VPB1001; Lonza). Briefly, HUAEC were trypsinized; suspended in the transfection solution with 300 nM si-ALK1, si-ALK3, si-BMPR2, si-ENG, si-SMAD4, or si-Cont; and electroporated using the Amaxa Nucleofector Device. At 36 h after transfection, cells were precultured in EBM-2 medium with 0.2% FBS for 3 h and treated with BMP9 or BMP10.

Subcellular Fractionation and ER Microsome Preparation. Subcellular fractionation of BMP9-treated HUAEC was performed using the ProteoExtract kit (Calbiochem), and ER microsome fractions were prepared using the Endoplasmic Reticulum Enrichment kit (Imgenex). TMEM100 and various marker proteins were detected by Western blot analysis.

Quantitative RT-PCR, Northern Blot Analysis, and in Situ Hybridization. Levels of mRNA expression were quantified using the SYBR green RT-PCR system (Qiagen). The PCR primers for human genes are as follows: *TMEM100*, 5′-CTTTCCCAGAAGTTGGACGA-3′ and 5′-CCTTGATGGGCTCTTCAGTC-3′; *ACVRL1/ALK1*, 5′-GTGGAGTGTGTGGGAAAAGG-3′ and 5′-TCATGTCTGAGGCGATGAAG-3′; *ACVR1/ALK2*, 5′-GAAGGGCTCATCACCACCAAT-3′ and 5′-GAACGGTGGCTTGTAATCCTC-3′; *BMPR1A/ALK3*, 5′-TGGGCCTTGCTGTTAAATTC-3′ and 5′-ATTCTTCCACGATCCCTCCT-3′; *BMPR1B/ALK6*, 5′-ACACCACAGGGCTTTACTTAT-3′ and 5′-AATTGCTGGTTTGCCTTGAGT-3′; *BMPR2*, 5′-TGGCAGTGAGGTCACTCAAGG-3′ and 5′-GTTGCGTTCATTCTGCATAGC-3′; *ENG*, 5′-CACTAGCCAGGTCTCGAAGGG-3′ and 5′-CTGAGGACCAGAAGCACCTC-3′; *GAPDH*, 5′-ACCACAGTCCATGCCATCAC-3′ and 5′-TCCACCACCCTGTTGCTGTA-3′; *TGFBR1/ALK5*, 5′-GATGGGCTCTGCTTTGTCTC-3′ and 5′-CAAGGCCAGGTGATGACTTT-3′; and *TGFBR2*, 5′-ATGAGCAACTGCAGCATCAC-3′ and 5′-GGAGAAGCAGCATCTTCCAG-3′.

The PCR primers for mouse genes are as follows: *Tmem100*, 5′-TTCTGTGAGCTTGCATCCTG-3′ and 5′-CCGTGGTGACCACAACTTC-3′; *Cdh5*, 5′-TCAACGCATCTGTGCCAGAGAT-3′ and 5′-CACGATTTGGTACAAGACAGTG-3′; *Efnb2*, 5′-AGGAATCACGGTCCAACAAG-3′ and 5′-GTCTCCTGCGGTACTTGAGC-3′; *eNOS/Nos3*, 5′-CCTTCCGCTACCAGCCAG-3′ and 5′-CAGAGATCTTCACTGGATTGGCT-3′; *Ephb4*, 5′-GGTCAGCGCTCTGGACAAGATG-3′ and 5′-AGCCGAATCCAGCCGCTGCAA-3′; *Gja4/Cx37*, 5′-AGTGCCTCAGACCCTTACC-3′ and 5′-GAGTGACATTAGCCCCAGAT-3′; *Gja5/Cx40*, 5′-AGAGCCTGAAGAAGCCAACT-3′ and 5′-GGCGTGGACACAAAGATGA-3′; *Hes5*, 5′-GCAGCATAGAGCAGCTGAAG-3′ and 5′-TAGTCCTGGTGCAGGCTCTT-3′; *Hrt1/Hey1*, 5′-CTGAGCTGAGAAGGCTGGTACC-3′ and 5′-ACCCCAAACTCCGATAGTCC-3′; *Hrt2/Hey2*, 5′-GAGAAGACTAGTGCCAACAGC-3′ and 5′-GCATGGGCATCAAAGTAGCCT-3′; *Kdr/Flk1*, 5′-CGCTTTTGGAATTGACAAGACA-3′ and 5′-ACCAATGTGGATGAGGATCTTGA-3′; *Klf2*, 5′-CCAAGAGCTCGCACCTAAAG-3′ and 5′-GTGGCACTGAAAGGGTCTGT-3′; *Notch1*, 5′-CTGACGCCCTTGCTCTGCCTAA-3′ and 5′-AGTGCCACCATGGTCCACAACG-3′; *Notch4*, 5′-AGGCTGGAGCGGATAAAGAT-3′ and 5′-CTTCCAGCAGCGTTAGCAG-3′; and *Pecam1*, 5′-AACAGAAACCCGTGGAGATG-3′ and 5′-GTCTCTGTGGCTCTCGTTCC-3′.

Quantitative RT-PCR for *18S* ribosomal RNA, *Hes1*, and *Hrt3* was performed using TaqMan probe assays (Applied Biosystems). Ten micrograms each of total RNA from whole embryos and adult tissues of C57BL/6 mice was applied to Northern blot analysis, using 1.7-kb mouse *Tmem100* cDNA fragments as a probe template. Information of digoxigenin-labeled RNA probes for in situ hybridization is available upon request.

***Alk1/Acvrl1* Knockout Mice.** *Acvrl1/Alk1* knockout mouse line B6.129P2-*Acvrl1*^{tm1Dgen}/J was obtained from the Jackson Laboratory.

Generation of Endothelial-Specific *Tmem100* Knockout Mice. Conditional deletion of *Tmem100* in an endothelial-specific manner was done using the Cre/loxP recombination system. The targeting vector (Fig. S8*A*) was constructed to insert loxP sequences to the sites flanking the protein-coding region in exon 3. The PGK-neo cassette was removed by breeding with *CAG-FLP* transgenic mice. *Tek-Cre* transgenic mice were used for breeding to generate endothelial-specific *Tmem100* knockout mice (1). Maintenance breeding was done with the mice under the C57BL/6 genetic background.

Genotyping of Mice with *Tmem100* Null and Conditional *Tmem100* Knockout Alleles. The targeting strategy to generate the *Tmem100* null allele is shown in Fig. S3*A*. HpaI-StuI and HindIII digestions of genomic DNA were used for Southern blot analysis with 5′ and 3′ probes, respectively (Fig. S3*B*). PCR primers for genotyping are as follows: F1 (5′-CTTGCATCCTGACCAGGCTTTCC-3′) and R1 (5′-CACAGCGGTGACCACAATCCCAG-3′) for amplification of the wild-type allele and F1 and R2 (5′-CTCTTCGCTATTACGCCAGCTGG-3′) for the null allele (Fig. S3*C*).

The conditional targeting strategy of *Tmem100* is shown in Fig. S8*A*. ApaI and SpeI digestions of genomic DNA were used for Southern blot analysis with 5′ and 3′ probes, respectively (Fig. S8*B*). PCR primers for genotyping are as follows; F1 (5′-AAAGGAACAAGAAAGTCAAGAGACG-3′) and R1 (5′-AGTTCACTGAGTTAGAGCAGTGTGG-3′) for amplification of the wild-type and *floxed* alleles and F2 (5′-ATGTCTCCCACCTTCTTCTTCACAG-3′) and R2 (5′-GGTACATCAGGTGGACCTCTCTT-3′) for the *floxed* and *deleted* alleles (Fig. S8 *C* and *D*).

Statistical Analysis. Results are expressed as the means ± SD. Student's *t* tests were used to analyze differences between two groups. Within-group differences and between-group differences following treatments were assessed with one-way ANOVA and two-way ANOVA, respectively. Significant differences were defined as P values <0.05.

1. Kisanuki YY, et al. (2001) Tie2-Cre transgenic mice: A new model for endothelial cell-lineage analysis in vivo. *Dev Biol* 230:230–242.

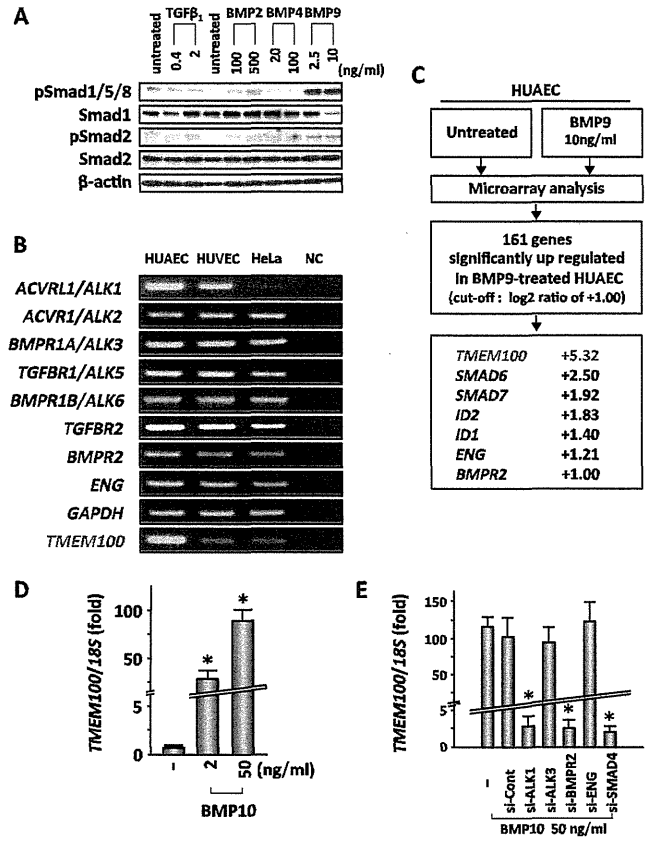

Fig. S1. Microarray analysis to identify BMP9/BMP10-dependent genes in endothelial cells. (*A*) BMP9, but not TGF-β1, BMP2, and BMP4, stimulates Smad1/5/8 phosphorylation in human umbilical artery endothelial cells (HUAEC) at 1 h of treatment. pSmad indicates phosphorylated Smad. Western blot analysis is shown. (*B*) *ACVRL1/ALK1* is expressed abundantly in HUAEC compared with human umbilical vein endothelial cells (HUVEC) and HeLa cells. *TMEM100* mRNA is also enriched in HUAEC. The genes encoding other type I ALK receptors, type II receptors, and Endoglin show similar expression levels. NC, negative control without cDNA. RT-PCR is shown. (*C*) A microarray analysis was performed using the BMP9-treated and untreated HUAEC. The list comprises up-regulated genes in BMP9-stimulated HUAEC (cutoff: log2 ratio of +1.00). (*D*) Not only BMP9 but also BMP10 induces *TMEM100* mRNA expression in HUAEC. Quantitative RT-PCR analysis is shown. –, untreated. (*E*) BMP10-induced *TMEM100* mRNA expression is inhibited by the pretreatment with ACVRL1/ALK1 siRNA (si-ALK1), BMPR2 siRNA (si-BMPR2), or SMAD4 siRNA (si-SMAD4), but not with BMPR1A/ALK3 siRNA (si-ALK3), Endoglin siRNA (si-ENG), or control siRNA (si-Cont). Quantitative RT-PCR is shown. –, untreated.

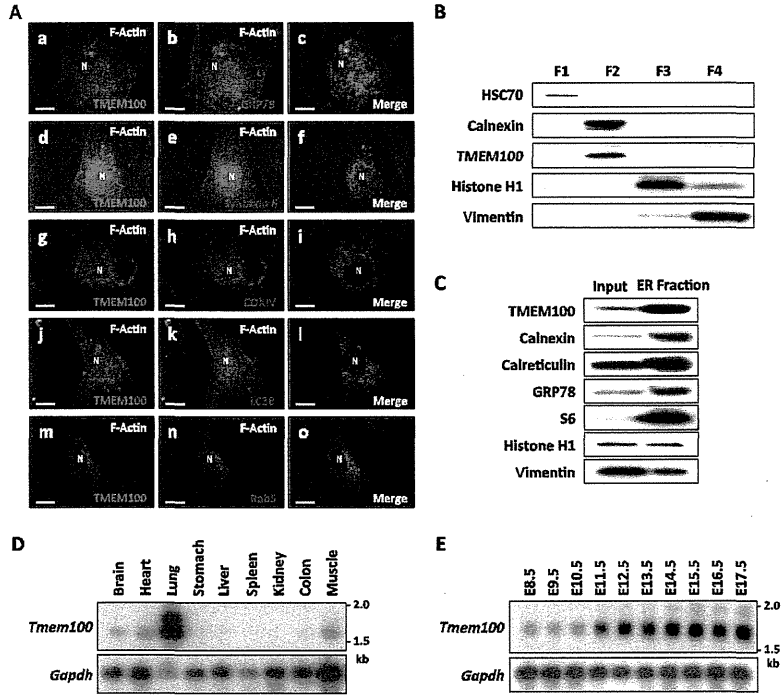

Fig. S2. Subcellular localization of TMEM100 protein and expression profiles of *Tmem100* in mice. (*A*) TMEM100 protein is colocalized with an endoplasmic reticulum (ER) protein, GRP78/HSPA5, but not with other organelle markers, including Syntaxin 6 (for Golgi), COXIV (mitochondria), LC3B (autophagosome), and Rab5 (endosome). Shown is immunocytochemistry of HUAEC transfected with a TMEM100-FLAG expression plasmid. N, nucleus. (*B*) Endogenous TMEM100 protein is recovered to the membrane fraction (F2) from BMP9-treated HUAEC, but not to the cytosolic (F1), nucleic (F3), and cytoskeleton (F4) fractions. HSC70, Calnexin, Histone H1, and Vimentin are used as positive controls for F1–F4 fractions, respectively. Western blot analysis is shown. (*C*) TMEM100 protein is enriched in the ER microsome fraction, which is also observed for representative ER-enriched proteins. Histone H1 and Vimentin levels are shown as negative controls. Western blot analysis using BMP9-treated HUAEC is shown. (*D*) *Tmem100* is expressed predominantly in the lung of adult mice and in the brain, heart, and muscle at lower levels. Northern blot analysis is shown. (*E*) *Tmem100* is expressed in mouse embryos from E8.5, with higher levels observed at later stages. Northern blot analysis is shown. *Gapdh* expression is shown as a control. (Scale bars in *A*, 10 μm.)